UNIVERSITÄT HAMBURG

UNIVERSITÀ DEGLI STUDI
DELL'AQUILA

UNIVERSITAT AUTÒNOMA DE
BARCELONA

Erasmus Mundus Consortium
MathMods

Joint Degree of Master of Science in
Mathematical Modelling in Engineering: Theory, Numerics, Applications

In the framework of the
Consortium Agreement and Award of a Joint/Multiple Degree 2013-2019

Master's Thesis

Aqueous Humor Flow in the Posterior Chamber of the Eye in the Cases of Iridotomy and Implanted Hole-ICL

ADVISORS:

Prof. Rodolfo Repetto **Prof. Pierangelo Marcati** **Dr. Jennifer H. Siggers**

CANDIDATE:

Mariia Dvoriashyna
Matricola: **228483**

2014/2015

Dipartimento di Ingegneria e Scienze dell'Informazione e Matematica
Laurea Magistrale in Ingegneria Matematica
Università degli Studi dell'Aquila

"When there is a difficulty in describing something with words, one uses mathematics."

UNIVERSITY OF L'AQUILA

Abstract

Department of Information Engineering, Computer Science and Mathematics

Master of Science

Aqueous Humor Flow in the Posterior Chamber of the Eye in the Cases of Iridotomy and Implanted Hole-ICL

by Mariia Dvoriashyna

The present work describes a mathematical model of the aqueous flow in the posterior chamber of the eye in a presence of iridotomy (i.e. a hole in the iris created with a surgery and aimed at reducing the intraocular pressure) and implanted artificial intraocular lens (Hole-ICL). A first goal of the model is to predict the pressure distribution in the posterior chamber with an iridotomy and find a dependence of the flux through the iridotomy on the size and location of the hole. Since the fluid domain is long and thin, we use the lubrication theory to simplify the Navier-Stokes equations. We assume that the flux through the holes is proportional to the pressure drop and model the iridotomy holes as point sinks. To this end, we work in terms of a suitably regularised pressure. The semi-analytical solution for the pressure and velocity is obtained for realistic shapes of the posterior chamber, which are inferred from ultrasound scan images. The results allow us to predict the ideal size of the iridotomy that is sufficient to keep the pressure within safe limits and also avoid large velocities to be generated. A second aim of the work is to study how the fluid flow changes after implantation of a Hole-ICL intraocular lens. This is an artificial lens that it is implanted in the posterior chamber and has a hole in its body to allow fluid passage. Our simulations show that, for the size of the hole that is employed in commercially available lenses, most of the fluid flow takes place through the hole in the lens and very little through the ICL-iris channel.

Acknowledgements

I would like to express my deep gratitude to my research supervisors Prof. Rodolfo Repetto, Dr. Jennifer H. Siggers and Prof. Pierangelo Marcati, for their patient guidance, enthusiastic encouragement, valuable advices and useful critiques of this research work. Their guidance helped me in all the time of writing of this thesis. I would like to offer my special thanks to Prof. Bruno Rubino and Prof. Corrado Lattanzio for all their coordination and help during my studies in *MathMods*. My sincere thanks also goes to Paolo Soleri and Opthec BV for offering this project and providing useful comments. I wish to acknowledge the help provided by Dr. Mario Romano, who explained the problem from medical point of view and provided medical images of the eye. I am particularly grateful for the assistance and favorable suggestions given by Peyman Davvalo Khongar and Masoud Ghaderi Zefreh. The studies in *MathMods* would have been impossible for me without the support of Erasmus Mundus scholarship. Finally, I wish to thank Yaroslava Gerfanova, Miriam Srokova, Mariia Koroliuk and my parents for their support and encouragement throughout my study.

Contents

List of Figures

Constants and Notations

Height of the posterior chamber at the ciliary body	h_0	=	$0,7275$ mm
Height of the posterior chamber at the pupil	h_i	=	7 μm
Radius of the pupil	r_p	=	$2,5$ mm
Radius of the posterior chamber	r_{pc}	=	$6,3$ mm
Thickness of the iris	S, S_i	=	$0,406$ mm
Flux produced by ciliary body	F	=	3 μl/min
Dynamic viscosity of aqueous humor	μ	=	$0,75$ g/m$\cdot s$
Density of aqueous humor	ρ	=	$994,7$ kg/m^3
Thickness of ICL in place of the hole	S_l	=	50 μm
Radius of ICL	r_l	=	$4,5$mm
Radius of the hole in ICL	r_0	=	$0,36$mm

Chapter 1

Introduction

1.1 The aqueous humour

The aqueous humour is a transparent fluid with mechanical properties similar to those of water, and containing proteins in small concentration. It occupies the anterior and posterior chambers of the eye, the spaces between the lens and the cornea (fig. 1.1). The aqueous humour is produced at a constant rate in correspondence of the ciliary muscle, the structure supporting the lens, it flows in the posterior chamber, passes through the pupil into the anterior chamber and is finally drained in correspondence of the trabecular meshwork. The aqueous humor flow has many physiological functions, among which the most important are:

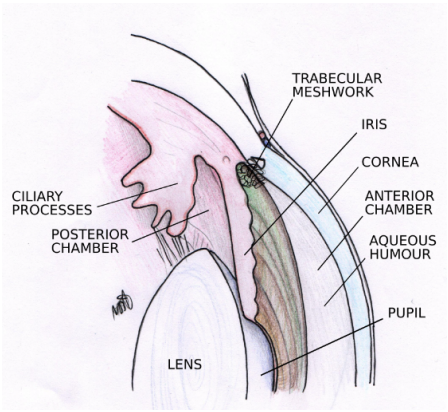

FIGURE 1.1: Sketch of a vertical cross-section of the eye.

- maintaining the intraocular pressure (pressure within the eye) and inflating the globe of the eye;
- providing nutrition to the avascular tissues of the cornea and lens (e.g. amino acids and glucose);

- transporting ascorbate in the anterior segment to act as an antioxidant agent.

1.1.1 Mechanisms that drive the aqueous flow

The main mechanisms that generate flow of the aqueous humor are:

- production at the ciliary processes and drainage at the trabecular meshwork;
- miosis, i.e. contraction of the pupil;
- temperature differences between the anterior and the posterior regions of the anterior chamber. This temperature gradient produces a thermal flow, i.e. a flow induced by buoyancy effects;
- motion induced by saccades (quick movements) of the eye.

A relatively large number of studies have been published in this field. Below, some of the main contributions concerning the fluid mechanics of the aqueous are recalled and briefly described. Heys et al. [2] studied fluid flow production and drainage assuming that iris is an elastic solid. Canning et al. [3] used lubrication theory to find analytical solutions for the natural convection in the anterior chamber. Modarreszadeh et al. [4] and Abouali et al. [5] investigated the effects of eye rotations on the flow of aqueous numerically. Silver [6] considered the aqueous flow in the iris-lens channel. A comprehensive and relatively up to date review of the fluid mechanics of the eye and, in particular, of aqueous flow is given in Siggers and Ethier (2012, [7]). In the present work we investigated the flow of aqueous humor in the posterior chamber, in particular the flow due to aqueous humor production and due to miosis.

1.2 Glaucoma

Glaucoma is a condition characterised by progressive death of retinal ganglion cells. It is very often associated with an increased intraocular pressure. This can happen either through an increased production or an increased resistance to aqueous humour outflow. Increased resistance to outflow of aqueous humour may occur due to an abnormal trabecular meshwork or to obliteration of the meshwork due to injury or disease of the iris. There are two main kinds of glaucoma: open-angle and closed-angle. In open/wide-angle

glaucoma, resistance growth in the trabecular meshwork due to degeneration and obstruction of the meshwork, whose original function is to drain the aqueous humor. This leads to a chronic, painless buildup of the pressure in the eye. In close/narrow-angle, the iridocorneal (between cornea and iris) angle is completely closed owing to a forward displacement of the iris against the cornea, which is tipically caused by pupillary block. This results in the inability of the aqueous fluid to flow from the posterior to the anterior chamber and then out of the trabecular meshwork. This accumulation of aqueous humor causes an acute increase of pressure and pain. For this case immediate surgical treatment is necessary. There is a common procedure for it, which is called iridotomy. It consists in producing a hole in the iris, thus reducing the resistance to flow from the posterior to the anterior chamber. The procedure is usually done with laser, and the hole is placed in the iris under the upper eyelid at the 12-o'clock position (or at 3- or 9-o'clock positions depending on surgeon preference). The typical size of the iridotomy, according to Silver et al. [6], is 100μm in diameter.

In chapter 3 of this thesis a theoretical model of aqueous flow in the posterior chamber in the presence of iridotomy is described. For the current work we used lubrication theory for simplifying the equations, which is applicable since the posterior chamber is long and thin. The reason for choosing the theoretical model rather than numerical one is that the channel between iris and the lens in very thin ($\sim 7\mu$m) and it causes the error in numerical models in terms of flux conservation. To our best knowledge this is the first mathematical study of the flow in the posterior chamber and also the first study concerning the role of iridotomy.

The aim of the present work is to investigate the influence of the iridotomy on the aqueous flow in the posterior chamber of the eye. We want to look for the dependence between the outflow from the iridotomy and the size of the hole, to find the pressure drop and velocity distribution in the posterior chamber.

1.3 Intraocular lenses

Phakic intraocular lenses (pIOLs) are artificial lenses that are implanted in the eye without removing or altering the natural crystalline lens. Surgical interventions for refractive error correction have become a viable alternative to the wearing of spectacles and contact lenses. The most commonly adopted option is laser surgical remodeling of the cornea; however, eyes with insufficient corneal thickness or very high refraction errors are unsuitable for this surgery, but may be treated by the implantation of an artificial

intraocular lens. There are three main types: sulcus-supported lenses are placed in the posterior chamber, while angle-supported lenses and iris-fixated lenses are placed in the anterior chamber. Although there are many advantages of Phakic IOLs, they might be also associated with some possible complications, which, according to Kwitko and Stolz [8] include loss of endothelial cells from the cornea, cataract formation, secondary glaucoma, iris atrophy, and dislocation. Many works are devoted studying these kind of lenses and their effect on the fluid flow in human eye. Baumeister et al. [9] evaluated the distance between the phakic IOL and the crystalline lens and the cornea as well as rotation around the optical axis for all three types of pIOLs. Kohnen et al. [10] overwied possible complications due to the pIOL implantation. Repetto et al. [11] studied the fluid flow in the anterior chamber in the presence of iris-fixated lens using numerical techniques. Kawamorita [1] performed numerical simulations considering the aqueous circulation with the sulcus-supported lenses in the posterior chamber. In the present work we will focus in the special type of posterior chamber phakic intraocular lenses Hole-ICL.

1.3.1 Hole-ICL

Posterior chamber (PC) phakic intraocular lenses (pIOLs) have many advantages for the treatment of refractive error. The toric implantable collamer lens (ICL) has been observed to be effective for the correction of miopia [12], [13]. However, cataract development has been noted after PC pIOL implantation by Chen et al. [14]. Authors made a systematic literature overview to determine the case of cataracts after the implantation of pIOL, and to identify the possible factors for cataract formation. They reported the incidence of the formation of cataract to be 9.6%, and the study of cataract progression in eyes with pre-existing cataracts presented a progression rate of 29.5% after pIOL surgery. The cause of secondary cataracts may be a change in the aqueous humor flow around the crystalline lens. Therefore, a centrally perforated ICL (i.e., the Hole-ICL) was created to improve aqueous humour circulation (see figure 1.2). The improvement

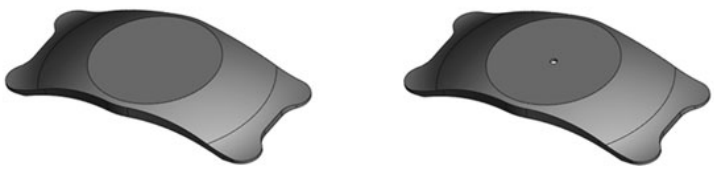

FIGURE 1.2: On the left - toric ICL, centrally perforated ICL on the right ([1])

of aqueous flow in porcine eyes was observed by Fujisawa [15], who concluded that the

Hole-ICL allowed sufficient flow of aqueous humor around the anterior surface of natural crystalline lens. However, the circulation of aqueous humour in a porcine eye would be different from that in a human eye. In 2012 Kawamorita et al. [1] studied the fluid dynamics of aqueous humor with implanted Hole-ICL using computational fluid dynamics. In the present work (Chapter 4) we develop preliminary theoretical model using lubrication theory of aqueous flow in the posterior chamber of the eye. Although it the model is very simplified, there are some useful conclusions which we can obtain from the it. The aim is to determine the pressure drop and the velocity profile of aqueous humor in the posterior chamber of the eye with the Hole-ICL. The model allows us to vary geometrical parameters easily and to impose small values for iris-lens channel without loss of precision, which gives us an advantage over the numerical models.

Before the introduction of a hole in the body of ICL lenses their implantation was invariably accompanied by a laser iridotomy. This was done to provide an alternative path for the aqueous to flow from the posterior to the anterior chamber. With the introduction of Hole-ICL iridotomy is no more considered necessary. However, we test in Chapter 5 of this thesis the effect of an iridotomy in the case in which a Hole-ICL is implanted in the eye in order to check the changes in aqueous flow due to the iridotomy.

Chapter 2

Mathematical prerequisites

2.1 Lubrication Theory and simplification of the Navier-Sokes equations

Lubrication theory is a technique for simplifying the Navier-Srokes equations and obtaining an approximate solution of them. It applies to cases in which the domain is long and thin. We consider the posterior chamber to be an axisymmetric domain. The axis z passes through the center of the pupil. Let us consider the Navier-Stokes equations in cylindrical coordinates (r, θ, z):

$$\frac{1}{r}\frac{\partial(ru_r)}{\partial r} + \frac{1}{r}\frac{\partial u_\theta}{\partial \theta} + \frac{\partial u_z}{\partial z} = 0, \tag{2.1.1}$$

$$\begin{aligned}\frac{\partial u_r}{\partial t} + u_r\frac{\partial u_r}{\partial r} + \frac{u_\theta}{r}\frac{\partial u_r}{\partial \theta} - \frac{u_\theta^2}{r} + u_z\frac{\partial u_r}{\partial z} = \\ -\frac{1}{\rho}\frac{\partial p}{\partial r} + \nu\left(\frac{1}{r}\frac{\partial}{\partial r}\Big(r\frac{\partial u_r}{\partial r}\Big) - \frac{u_r}{r^2} + \frac{1}{r^2}\frac{\partial^2 u_r}{\partial \theta^2} - \frac{2}{r^2}\frac{\partial u_\theta}{\partial \theta} + \frac{\partial^2 u_r}{\partial z^2}\right)\end{aligned} \tag{2.1.2}$$

$$\begin{aligned}\frac{\partial u_\theta}{\partial t} + u_r\frac{\partial u_\theta}{\partial r} + \frac{u_\theta}{r}\frac{\partial u_\theta}{\partial \theta} + \frac{u_r u_\theta}{r} + u_z\frac{\partial u_\theta}{\partial z} = \\ -\frac{1}{\rho r}\frac{\partial p}{\partial \theta} + \nu\left(\frac{1}{r}\frac{\partial}{\partial r}\Big(r\frac{\partial u_\theta}{\partial r}\Big) - \frac{u_\theta}{r^2} + \frac{1}{r^2}\frac{\partial^2 u_\theta}{\partial \theta^2} + \frac{2}{r^2}\frac{\partial u_r}{\partial \theta} + \frac{\partial^2 u_\theta}{\partial z^2}\right)\end{aligned} \tag{2.1.3}$$

Radius of the pupil	r_p	2.5 mm
Radius of the ciliary body	r_{pc}	6.3 mm
Height of the chamber on the outer boundary	h_0	0.727 mm
Height of the iris-lens channel	h_i	7 μm
Flux produced by ciliary body	F	3 μl/min
Dynamic viscosity of aqueous humor	μ	0.75 g/m/s

TABLE 2.1: Geometrical values and fluid properties

$$\frac{\partial u_z}{\partial t} + u_r\frac{\partial u_z}{\partial r} + \frac{u_\theta}{r}\frac{\partial u_z}{\partial \theta} + u_z\frac{\partial u_z}{\partial z} = \\ -\frac{1}{\rho}\frac{\partial p}{\partial z} + \nu\left(\frac{1}{r}\frac{\partial}{\partial r}\Big(r\frac{\partial u_z}{\partial r}\Big) + \frac{1}{r^2}\frac{\partial^2 u_z}{\partial \theta^2} + \frac{\partial^2 u_z}{\partial z^2}\right) \quad (2.1.4)$$

where $\mathbf{u} = (u_r, u_\theta, u_z)$ is the velocity vector and p is the pressure. Moreover, ρ denotes fluid density and ν fluid viscosity. We denote with r_p is the radius of the pupil and with r_{pc} the distance from the centre of the pupil to the outer boundary of the posterior chamber (see figure 2.1). Thus, in the radial direction the domain extends from r_p to r_{pc} ($r_p < r < r_{pc}$). The height of the posterior chamber is a decreasing function $h(r)$ (from now on the height of the domain is given by the function obtained from the realistic geometry, the details can be found in § 3.3). Let $L = r_{pc} - r_p \approx 4.8$ mm be the radial length of the domain. We define the average height of the domain $h_a = \frac{1}{L}\int_{r_p<r<r_{pc}} h(r)dr \approx 0.44$ mm. Let us introduce the ratio $\epsilon = h_a/L = 0.092 << 1$. Thus, we can state that the domain is long and thin and we can apply lubrication theory.

We assume that changes in the r and θ velocity components u_r and u_θ are of order of U, thus $|\Delta u_r| \sim |\Delta u_\theta| \sim U$. Then, derivatives of the velocities with respect to the r and θ directions can be estimated as $|\frac{\partial u_r}{\partial r}| \sim |\frac{1}{r}\frac{\partial u_\theta}{\partial \theta}| \sim U/L$. From the continuity equation (2.1.1) we obtain the order of $|\frac{\Delta u_z}{\Delta z}| \sim U/L$, hence $|\Delta u_z| \sim h_a U/L$. In the next section we will rescale and simplify the Navier-Stokes equations (2.1.1)-(2.1.4) using lubrication theory.

2.2 Scaling

Let us consider U to be a characteristic scale for the velocity. We will discuss in the following how U is defined, depending on the case under consideration.

Let us introduce the following scales:
$r = Lr^*$, $z = h_a z^*$, $h(r) = h^*(r^*)h_a$, $u_r = Uu_r^*$, $u_\theta = Uu_\theta^*$, $u_z = \frac{Uh_a}{L}u_z^*$. The scale for

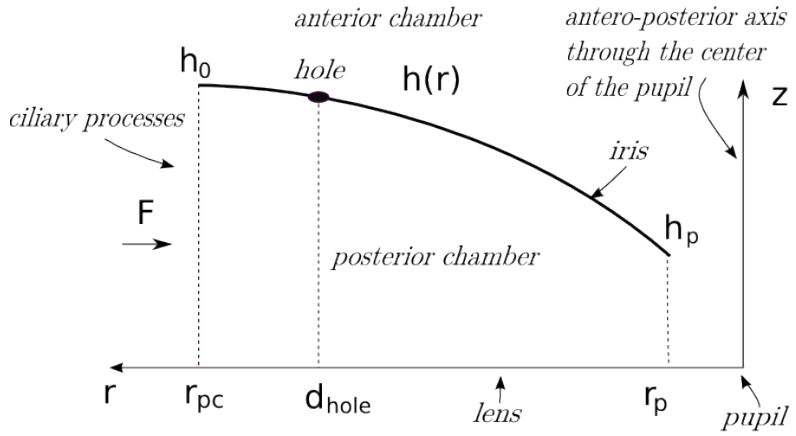

FIGURE 2.1: Sketch of the vertical cross-section of the domain

the pressure $p = p^* \frac{L\mu U}{h_a^2}$ is obtained by balancing the pressure derivative with the leading viscous terms.

2.2.1 Flow due to aqueous production

The flow due to the aqueous production is steady, thus we can drop the term with the time derivative from the equations. Let us scale the velocity through the incoming flux produced by ciliary body, which is known to be approximately constant (see 2.1), $U = F/2\pi r_{pc} h_0$. With the above scales we obtain the following dimensionless equations:

$$\frac{1}{r^*}\frac{\partial (r^* u_r^*)}{\partial r^*} + \frac{1}{r^*}\frac{\partial u_\theta^*}{\partial \theta} + \frac{\partial u_z^*}{\partial z^*} = 0, \tag{2.2.1}$$

$$\begin{aligned} Re\epsilon^2 \left(u_r^* \frac{\partial u_r^*}{\partial r^*} + \frac{u_\theta^*}{r^*}\frac{\partial u_r^*}{\partial \theta} - \frac{u_\theta^{*2}}{r^*} + u_z^* \frac{\partial u_r^*}{\partial z^*} \right) = \\ - \frac{\partial p^*}{\partial r^*} + \epsilon^2 \left(\frac{1}{r^*}\frac{\partial}{\partial r^*}\left(r^* \frac{\partial u_r^*}{\partial r^*} \right) - \frac{u_r^*}{r^{*2}} + \frac{1}{r^{*2}}\frac{\partial^2 u_r^*}{\partial \theta^2} - \frac{2}{r^{*2}}\frac{\partial u_\theta^*}{\partial \theta} \right) + \frac{\partial^2 u_r^*}{\partial z^{*2}} \end{aligned} \tag{2.2.2}$$

$$\begin{aligned} Re\epsilon^2 \left(u_r^* \frac{\partial u_\theta^*}{\partial r^*} + \frac{u_\theta^*}{r^*}\frac{\partial u_\theta^*}{\partial \theta} + \frac{u_r^* u_\theta^*}{r^*} + u_z^* \frac{\partial u_\theta^*}{\partial z^*} \right) = \\ - \frac{1}{r^*}\frac{\partial p^*}{\partial \theta} + \epsilon^2 \left(\frac{1}{r^*}\frac{\partial}{\partial r^*}\left(r^* \frac{\partial u_\theta^*}{\partial r^*} \right) - \frac{u_\theta^*}{r^{*2}} + \frac{1}{r^{*2}}\frac{\partial^2 u_\theta^*}{\partial \theta^2} + \frac{2}{r^{*2}}\frac{\partial u_r^*}{\partial \theta} \right) + \frac{\partial^2 u_\theta^*}{\partial z^{*2}} \end{aligned} \tag{2.2.3}$$

$$Re\epsilon^3\left(u_r^*\frac{\partial u_z^*}{\partial r^*}+\frac{u_\theta^*}{r^*}\frac{\partial u_z^*}{\partial \theta}+u_z^*\frac{\partial u_z^*}{\partial z^*}\right)= \\ -\frac{\partial p^*}{\partial z^*}+\epsilon^3\left(\frac{1}{r^*}\frac{\partial}{\partial r^*}\left(r^*\frac{\partial u_z^*}{\partial r^*}\right)+\frac{1}{r^{*2}}\frac{\partial^2 u_z^*}{\partial \theta^2}\right)+\epsilon\frac{\partial^2 u_z^*}{\partial z^{*2}} \quad (2.2.4)$$

where $Re = UL/\nu$ is the Reynolds number. The dimensionless number $\epsilon^2 Re$ is normally refered to in lubrication theory as reduced Reynolds number. With the chosen parameters we can estimate $\epsilon = 0.092$, $\epsilon^2 = 0.008$, $\epsilon^2 Re = 9.35 \cdot 10^{-5}$. These dimensionless numbers are small with respect to 1, thus we can neglect the terms of order $\epsilon, \epsilon^2, \epsilon^2 Re$ and obtain the following simplified equations:

$$\frac{1}{r^*}\frac{\partial (r^* u_r^*)}{\partial r^*}+\frac{1}{r^*}\frac{\partial u_\theta^*}{\partial \theta}+\frac{\partial u_z^*}{\partial z^*}=0 \quad (2.2.5)$$

$$\frac{\partial^2 u_r^*}{\partial z^{*2}}=\frac{\partial p^*}{\partial r^*} \quad (2.2.6)$$

$$\frac{\partial^2 u_\theta^*}{\partial z^{*2}}=\frac{1}{r^*}\frac{\partial p^*}{\partial \theta} \quad (2.2.7)$$

$$\frac{\partial p^*}{\partial z^*}=0 \quad (2.2.8)$$

2.2.2 Flow due to the miosis

For the case of miosis we will scale the velocity U as L/T, where $T = 1s$ (Repetto et al. [11]) is the time of the contraction and scale time $t = Tt^*$. With this scaling the equation (2.1.1) will become the same as (2.2.1) and the equations (2.1.2)-(2.1.4) will become duplicated (2.2.2)-(2.2.4) with the additional term corresponding to the time derivative $\epsilon^2 Re\frac{\partial \mathbf{u}}{\partial t}$. For this scenario the reduced Reynolds number is $\epsilon^2 Re = 0.25$. It is much bigger than in the previous case, however, it is still relatively small with respect to 1. Thus, as a first approach to the problem we still neglect the terms of the orders $\epsilon, \epsilon^2, \epsilon^2 Re$ to obtain the same simplified system, as (2.2.5)-(2.2.8). This justifies the quasi-steady approach which we will use to model the flow with miosis.

2.2.3 The equation for the pressure

Due to the equations obtained above, miosis can be modeled with the quasi-steady approach. Thus, we will model the iris motion by imposing the velocity distribution on the upper boundary of the domain but keeping the domain fixed. For convenience, we will describe here the equations that govern the flow due to the aqueous production as

a particular case of the flow due to miosis, in which the velocity at the boundary (the iris) is set equal to zero.

We assume that we have an axisymmetric motion of the iris, which we describe by imposing the velocity $\mathbf{v} = (v_r(r), 0, v_z(r))$. From the equation (2.2.8) we conclude that p does not depend on z. Thus, we can integrate the equations (2.2.6) and (2.2.7) with respect to z, applying no-slip boundary condition at $z = 0$ and the imposed velocity $\mathbf{v}$ at $z = h(r)$. We get the following equation for the velocity:

$$\mathbf{u}^* = -\frac{1}{2}\boldsymbol{\nabla}^* p^* z^* (h^* - z^*) + \frac{v_r^*}{h^*} z^* \tag{2.2.9}$$

In the equation the continuity equation (2.2.9) the pressure is still unknown. To determine it we integrate the continuity equation (2.2.5) with respect to z and using no-slip boundary condition at $z = 0$ and the velocity $\mathbf{v}$ at $z = h(r)$, we obtain the following equation for the pressure:

$$\boldsymbol{\nabla}^* \cdot (h^{*3} \boldsymbol{\nabla}^* p^*) = \frac{h^*}{2} \boldsymbol{\nabla}^* \cdot \mathbf{v}^* - v_r^* \cdot h^{*'} + v_z^*. \tag{2.2.10}$$

In the dimensional form this equation will become:

$$\frac{1}{12\mu} \boldsymbol{\nabla} \cdot (h^3 \boldsymbol{\nabla} p) = \frac{h}{2} \boldsymbol{\nabla} \cdot \mathbf{v} - v_r \cdot h' + v_z. \tag{2.2.11}$$

The boundary condition on the outer boundary of the posterior chamber is given by the flux F produced by ciliary body. We compute $\mathbf{q} = \int_0^{h(r)} \mathbf{u}\, dz = -\frac{h^3}{12\mu} \boldsymbol{\nabla} p + \frac{h v_r}{2}$. Therefore,

$$F = \oint_{r=r_{pc}} \mathbf{q} \cdot (-\hat{\mathbf{r}})\, dl = \oint_{r=r_{pc}} \frac{h^3}{12\mu} \frac{\partial p}{\partial r} - \frac{h}{2} v_r dl = \frac{2\pi h^3 r_{pc}}{12\mu} \frac{\partial p}{\partial r} - \pi h v_r r_{pc} \quad \text{on } r = r_{pc}. \tag{2.2.12}$$

The second boundary condition is the imposed pressure at the pupil, which we put to be equal to the reference value 0:

$$p = 0 \qquad \text{at } r = r_p. \tag{2.2.13}$$

Thus, using the lubrication theory we simplified the Navier-Stokes equations to the equation for the pressure (2.2.11) subject to the boundary conditions (2.2.12)-(2.2.13).

Chapter 3

Model of iridotomy

3.1 Assumptions and Model

Let us start with the description of the mathematical model of the iridotomy.

3.1.1 Assumptions

- **Geometry of iridotomy:** Where convenient we assume that the iridotomy diameter is small enough, so that the iridotomy can be modelled as a point hole through the iris.
- **Geometry of the posterior chamber:** We assume the posterior chamber has an axisymmetric height $h(r)$. The shape of the domain is taken from medical images, as described in §3.3.1.
- **Thermal effects:** We ignore thermal variations within the posterior chamber, as these are likely to be much smaller than those in the anterior chamber (in which thermal gradients drive the majority of the flow).
- **Fluid mechanics:** We treat the aqueous humour as an incompressible Newtonian fluid, which is a good approximation. We also neglect gravity (since it would only make a difference in the case of buoyant effects due to thermal differences). This means that the pressure has to be understood as the departure from the hydrostatic pressure distribution. Since the height of the posterior chamber is much less than that of the anterior chamber we assume that lubrication theory applies. This is also a good approximation.

- **Anterior chamber:** We assume the pressure in the anterior chamber is constant and set it equal to the reference value zero. Thus the pressures given in this section are relative to the (assumed constant) pressure in the anterior chamber.
- **Flow through the hole:** We use Dagan formula (based on [16]), which states that the volumetric flow of an incompressible Newtonian fluid through a circular hole in a flat membrane for low-Reynolds-number flows equals $a^4\pi\Delta p/(8S\mu + 3a\pi\mu)$, where a is the hole radius, S is the thickness of the surface, Δp is the pressure difference between points on either side of the hole and μ is the shear viscosity of the fluid.

3.1.2 Mathematical model

We consider a model of the posterior chamber with small holes representing iridotomies. Since the posterior chamber is long and thin, we apply lubrication theory and using the analysis in § 2.2.3 obtain the equation $\frac{1}{12\mu}\boldsymbol{\nabla}\cdot(h^3\boldsymbol{\nabla}p) = \frac{h}{2}\boldsymbol{\nabla}\cdot v_r - v_r\cdot h' + v_z$ for the flow in the posterior chamber. We assume there are N_h small holes, with the ith hole having polar coordinates (d_i, ϕ_i), radius a_i and a flux Q_i coming out of it. By the results of § 2.2 the velocity profile can be written as

$$\mathbf{u} = -\frac{1}{2\mu}\boldsymbol{\nabla}p \ \cdot z\ (h-z) + \frac{v_r z}{h}$$

from which we obtain the depth integrated velocity as

$$\mathbf{q} = \int_0^{h(r)} \mathbf{u}\, dz = -\frac{h^3}{12\mu}\boldsymbol{\nabla}p + \frac{hv_r}{2},$$

The volumetric flux through the hole i is given by

$$Q_i = \oint_{r_i=a_i} \mathbf{q}\cdot(-\hat{\mathbf{r}}_i)\, dl = \oint_{r_i=a_i} \frac{h^3}{12\mu}\frac{\partial p}{\partial r_i} - \frac{hv_r}{2} dl, \tag{3.1.1}$$

where r_i is the distance from the ith hole. Assuming that h is constant and equal to h_i and v_r is a constant around the border of the ith hole it follows that $\partial p/\partial r_i$ needs to have an average value of $6\mu Q_i/(\pi a_i h_i^3)$ around this border. By assuming the holes have zero size, we can solve on the simple geometry $r_p < r < r_{pc}$, where r_p is the pupil diameter and r_{pc} is the posterior chamber diameter. However, this approximation requires $\partial p/\partial r_i$ to tend to infinity at the hole. We define function $\hat{f} = \frac{6\mu Q_i}{\pi h_i^3}\ln\left(\frac{r_i}{a_i}\right)$ such that, $\partial\hat{f}/\partial r_i = 6\mu Q_i/(\pi a_i h_i^3)$. In this way $\hat{f}$ satisfies the flux requirement, therefore, we

subtract it from the pressure to regularise it. Hence we define a regularised pressure

$$p_{\mathsf{reg}} = p - \sum_{i=1}^{N_h} \frac{6\mu Q_i}{\pi h_i^3} \ln \frac{r_i}{a_i}. \tag{3.1.2}$$

If we assume Dagan's formula applies then $Q_i = a_i^4 \pi \Delta p_i / (8S\mu + 3a_i\pi\mu)$, where Δp_i is the pressure drop across the hole, and, assuming a uniform pressure in the anterior chamber, that we take to be the reference pressure of zero,

$$\Delta p_i = p_{\mathsf{reg}}|_i + \sum_{j=1, i\neq j}^{N_h} \frac{6\mu Q_j}{\pi h_j^3} \ln \frac{d_{ij}}{a_j}, \tag{3.1.3}$$

and therefore,

$$Q_i = \frac{\pi a_i^4}{8S\mu + 3\pi\mu a_i}\, p_{\mathsf{reg}}|_i + \sum_{j=1, i\neq j}^{N_h} \frac{6a_i^4 Q_j}{h_j^3(8S + 3\pi a_i)} \ln \frac{d_{ij}}{a_j}, \tag{3.1.4}$$

where d_{ij} is the distance between holes i and j. This can conveniently be written in a matrix notation as $\mathbf{MQ} = \mathbf{b}$, where $\mathbf{Q}$ is the vector of volumetric fluxes, $\mathbf{M}$ is a matrix of geometrical factors given by

$$M_{ij} = \begin{cases} 1 & \text{if } i = j \\ -\frac{6a_i^4}{h_j^3(8S+3\pi a_i)} \ln \frac{d_{ij}}{a_j} & \text{if } i \neq j, \end{cases} \tag{3.1.5}$$

and $\mathbf{b}$ is the vector given by $b_i = \frac{\pi a_i^4}{8S\mu + 3\pi\mu a_i}\, p_{\mathsf{reg}}|_i$. We therefore have the governing equation, written in terms of p_{reg}:

$$\begin{aligned} \frac{1}{12\mu}\boldsymbol{\nabla}\cdot\left(h^3\boldsymbol{\nabla}p_{\mathsf{reg}}\right) = -\sum_{i=1}^{N_h} \frac{Q_i}{2\pi h_i^3}\boldsymbol{\nabla}\cdot\left(h^3\boldsymbol{\nabla}\ln\frac{r_i}{a_i}\right) + \frac{h}{2}\boldsymbol{\nabla}\cdot v_r - v_r\cdot h' + v_z = \\ = -\sum_{i=1}^{N_h} \frac{Q_i}{2\pi r_i h_i^3}\frac{\partial h^3}{\partial r_i} + \frac{h}{2}\boldsymbol{\nabla}\cdot v_r - v_r\cdot h' + v_z. \end{aligned} \tag{3.1.6}$$

The boundary condition on the outer boundary of the posterior chamber is given by the flux F produced by ciliary body (2.2.12) and the condition at the pupil is given by an imposed pressure (2.2.13)

Therefore, we can rewrite the set of equations in terms of regularized pressure:

$$\boldsymbol{\nabla} \cdot \left(h^3 \boldsymbol{\nabla} p_{\mathsf{reg}}\right) = -\sum_{i=1}^{N_h} \frac{6\mu Q_i}{\pi r_i h_i^3} \frac{\partial h^3}{\partial r_i} + 12\mu\Big(\frac{h}{2}\boldsymbol{\nabla} \cdot v_r - v_r \cdot h' + v_z\Big) \tag{3.1.7}$$

subject to the boundary conditions:

$$Q_i = \frac{\pi a_i^4}{8S\mu + 3\pi\mu a_i}\, p_{\mathsf{reg}}|_i + \sum_{j=1, i\neq j}^{N_h} \frac{6a_i^4 Q_j}{h_j^3(8S + 3\pi a_i)} \ln\frac{d_{ij}}{a_j} \qquad \text{at the point } i,\ i = 1, ..., N_h\ , \tag{3.1.8}$$

$$\frac{\partial p_{\mathsf{reg}}}{\partial r} = \frac{6\mu F}{\pi r_{pc} h^3} + \frac{6\mu v_r}{h^2} - \sum_{1}^{N_h} \frac{6\mu Q_i}{\pi r_i h_i^3} \frac{\partial r_i}{\partial r} \qquad \text{flux boundary condition at } r = r_{pc}, \tag{3.1.9}$$

$$p_{\mathsf{reg}} = -\sum_{1}^{N_h} \frac{6\mu Q_i}{\pi h_i^3} \ln\frac{r_i}{a_i} \qquad \text{at the pupil } r = r_p, \tag{3.1.10}$$

with the unknowns p_{reg} and $Q_i, i = 1, ..., N_h$.

The relationship between the components of relative coordinate systems (r_i, θ_i) with the initial point in the hole (d_i, ϕ_i), and the coordinate system with the initial point at the center of the pupil (r, θ) are given by:

$$r_i = \sqrt{r^2 + d_i^2 - 2d_i r\cos(\theta - \phi_i)}, \qquad \theta_i - \phi_i = \tan^{-1}\left(\frac{r\sin(\theta - \phi_i)}{r\cos(\theta - \phi_i) - d_i}\right) \tag{3.1.11}$$

$$r = \sqrt{r_i^2 + d_i^2 + 2d_i r_i\cos(\theta_i - \phi_i)}, \qquad \theta - \phi_i = \tan^{-1}\left(\frac{r_i\sin(\theta_i - \phi_i)}{d_i + r_i\cos(\theta_i - \phi_i)}\right) \tag{3.1.12}$$

Thus we obtained mathematical model of the iridotomy.

3.2 Solutions

We will introduce two different methods for solving the equation that have been used in case of one hole and in case of multiple holes respectively. Both methods are based on the finite difference scheme.

3.2.1 Case of one hole

In the case of just one hole, we can rewrite the equation (3.1.7),

$$\boldsymbol{\nabla}\cdot\left(h^3\boldsymbol{\nabla}p_{\mathsf{reg}}\right) = -\frac{6\mu Q_{\mathsf{hole}}}{\pi r_{\mathsf{hole}}h_{\mathsf{hole}}^3}\frac{\partial h^3}{\partial r_{\mathsf{hole}}} + 12\mu\Big(\frac{h}{2}\boldsymbol{\nabla}\cdot v_r - v_r\cdot h' + v_z\Big) \tag{3.2.1}$$

where h_{hole} is the posterior chamber height at the hole and r_{hole} is the distance from the hole, subject to

$$Q_{\mathsf{hole}} = \frac{\pi a_i^4}{8S\mu + 3\pi\mu a_i}\, p_{\mathsf{reg}}|_{\mathsf{hole}} \qquad \text{at the hole,} \tag{3.2.2}$$

$$\frac{\partial p_{\mathsf{reg}}}{\partial r} = \frac{12\mu F}{2\pi r_{pc}h^3} + \frac{6\mu v_r}{h^2} - \frac{12\mu Q_{\mathsf{hole}}}{2\pi r_{\mathsf{hole}}h_{\mathsf{hole}}^3}\frac{\partial r_{\mathsf{hole}}}{\partial r} \qquad \text{flux boundary condition at } r = r_{pc}, \tag{3.2.3}$$

$$p_{\mathsf{reg}} = -\frac{12\mu Q_{\mathsf{hole}}}{2\pi h_{\mathsf{hole}}^3}\ln\frac{r_{\mathsf{hole}}}{a_{\mathsf{hole}}} \qquad \text{at the pupil,} \tag{3.2.4}$$

These equations should be solved for the unknowns p_{reg} and Q_{hole}. Assuming without loss of generality that the hole is on the positive x-axis at a distance d_{hole} from the centre of the pupil, then we have the following relationships (3.1.11) - (3.1.12):

$$r_{\mathsf{hole}} = \sqrt{r^2 + d_{\mathsf{hole}}^2 - 2d_{\mathsf{hole}}r\cos\theta}, \qquad \theta_{\mathsf{hole}} = \tan^{-1}\left(\frac{r\sin\theta}{r\cos\theta - d_{\mathsf{hole}}}\right)$$

$$r = \sqrt{r_{\mathsf{hole}}^2 + d_{\mathsf{hole}}^2 + 2d_{\mathsf{hole}}r_{\mathsf{hole}}\cos\theta_{\mathsf{hole}}}, \qquad \theta = \tan^{-1}\left(\frac{r_{\mathsf{hole}}\sin\theta_{\mathsf{hole}}}{d_{\mathsf{hole}} + r_{\mathsf{hole}}\cos\theta_{\mathsf{hole}}}\right), \tag{3.2.5}$$

where θ is the azimuthal angle and θ_{hole} is the azimuthal angle from the hole, and therefore

$$\frac{\partial r_{\mathsf{hole}}}{\partial r} = \frac{r - d_{\mathsf{hole}}\cos\theta}{r_{\mathsf{hole}}}.$$

Let us solve the system using finite difference method. Consider the domain in the polar coordinates $D = \{r_p \le r \le r_{pc}\}$. On D let us introduce the uniform partition in θ and non uniform in r:

$$\omega = \{(r_i,\theta_i)\in D,\ r_i = r_{i-1} + s_{i-1},\ \theta_i = \theta_{i-1} + s_\theta,\ r_0 = r_p, r_{n_r} = r_{pc},\ \theta_0 = 0, \theta_{n_\theta} = 2\pi\}.$$

In order to define the step s_r we put the shape of the grid to be squares, such that $s_i = r_i s_\theta$. Then, the average step $\hat{s}$ we will define as

$$\hat{s}(i) = \begin{cases} \frac{1}{2}s_0 & \text{if } i = 0, \\ \frac{1}{2}(s_i + s_{i-1}) & \text{if } 1 \le i \le n_r - 1, \\ \frac{1}{2}s_{n_r-1} & \text{if } i = n_r. \end{cases}$$

Let us introduce the grid function $\rho(i)$:

$$\rho(i) = \begin{cases} r_p + \frac{1}{4}s_0 & \text{if } i = 0, \\ r_i + \frac{1}{4}(s_i - s_{i-1}) & \text{if } 1 \le i \le n_r - 1, \\ r_{pc} - \frac{1}{4}s_{n_r-1} & \text{if } i = n_r. \end{cases}$$

Since we have two unknowns p_{reg} and Q_{hole} which are connected by the boundary condition at the point of the hole (3.2.2), we will replace Q_{hole} in the equations using this formula. Thus, we need to solve the problem for p_{reg} only and then apply the condition (3.2.2) to find the flux through the hole.

Let us define the following functions

$$a(r) = rh^3 \qquad c(r,\theta) = \frac{6\pi a_{\mathsf{hole}}^4}{(8S + 3\pi a_{\mathsf{hole}}) r_{\mathsf{hole}} h_{\mathsf{hole}}^3} \frac{\partial h^3}{\partial r_{\mathsf{hole}}}$$

$$b(r) = h^3 \qquad f(r,\theta) = 12\mu\Big(\frac{h}{2}\boldsymbol{\nabla}\cdot v_r - v_r \cdot h' + v_z\Big)$$

$$g^{(2)} = -\frac{6\mu F}{\pi r_{pc}} + 6\mu v_r h \qquad g^{(1)}(\theta) = \frac{3a_{\mathsf{hole}}^4}{(8S + 3\pi a_{\mathsf{hole}}) h_{\mathsf{hole}}^3} \ln\left(\frac{r_p^2 + d_{\mathsf{hole}}^2 - 2d_{\mathsf{hole}} r_p \cos\theta_j}{a_{\mathsf{hole}}^2}\right)$$

$$g^{(3)}(\theta) = \frac{6a_{\mathsf{hole}}^4 h^3}{(8S + 3\pi a_{\mathsf{hole}}) r_{\mathsf{hole}} h_{\mathsf{hole}}^3} \frac{\partial r_{\mathsf{hole}}}{\partial r}.$$

Moreover, let us denote $a_i^+ = a(r_{i+1/2})$, $a_i^- = a(r_{i-1/2})$, where $r_{i+1/2} = r_i + s_i/2$, $r_{i-1/2} = r_i - s_{i-1}/2$. For the discretized functions at the points of the grid ω we will use the notation with indexes, i.e.

$$a_i = a(r_i) \qquad b_i = b(r_i) \qquad c_{i,j} = c(r_i, \theta_j)$$

$$f_{i,j} = f(r_i, \theta_j) \qquad g_j^{(1)} = g^{(1)}(\theta_j) \qquad g_j^{(3)} = g^{(3)}(\theta_j).$$

and the unknown function we denote y. Let us define i^* to be the point in radial direction of the grid ω which is closest to the point of the hole. Since we placed the hole in positive x-axis, the point closest to the hole in ω will be $(r_{i^*}, 0)$. We will use second order finite difference method for the non-uniform grid. The scheme is taken from the

book by Samarsky and Nikolaev [17] (available in russian only). The equation (3.2.1) will become:

$$\frac{1}{\rho\hat{s}}\left(\frac{a_i^-}{s_{i-1}}y_{i-1,j}-\left(\frac{a_i^-}{s_{i-1}}+\frac{a_i^+}{s_i}\right)y_{i,j}+\frac{a_i^+}{s_i}y_{i+1,j}\right)+\frac{b_i}{\rho^2}\,\frac{y_{i,j-1}-2y_{i,j}+y_{i,j+1}}{s_\theta^2}+$$
$$+c_{i,j}y_{i^*,0}=f_{i,j},\quad 1\le i\le n_r-1,\ 0\le j\le n_\theta-1. \quad (3.2.6)$$

We also take into account periodicity condition:

$$y(i,j)=y(i,j+n_\theta), j=0,-1. \quad (3.2.7)$$

The boundary condition at the pupil (3.2.4) can be written as

$$y_{0,j}+g_j^{(1)}y_{i^*,0}=0,\quad 0\le j\le n_\theta-1 \quad (3.2.8)$$

To discretize (3.2.3) we use "ghost" point method:

$$-\frac{a_{n_r}^-}{\rho\hat{s}s_{n_r-1}}(y_{n_r,j}-y_{n_r-1,j})+\frac{b_{n_r}}{\rho^2}\cdot\left(\frac{y_{n_r,j-1}-2y_{n_r,j}+y_{n_r,j+1}}{s_\theta^2}\right)+c_{n_r,j}y_{i^*,0}-$$
$$-\frac{a_{n_r}^-}{\rho\hat{s}}g_j^{(3)}y_{i^*,0}=f_{n_r,j}-\frac{r}{\rho\hat{s}_{n_r}}g^{(2)}\quad 0\le j\le n_\theta-1, \quad (3.2.9)$$

Therefore, we obtained $(n_r+1)n_\theta$ equations for $(n_r+1)n_\theta$ unknowns $y_{i,j}$. Solving the system directly requires lots of memory, since the dimension of the matrix is $(n_r+1)^2\cdot n_\theta^2$. Thus, in order to reduce the computational complexity and speed up the calculations we will use the modified method of reduction.

We put our system into the following vector form:

$$-\boldsymbol{Y}_{j-1}+C\boldsymbol{Y}_j-\boldsymbol{Y}_{j+1}+D_j\boldsymbol{Y}_0=\boldsymbol{F}_j,\quad 1\le j\le N-1$$
$$-\boldsymbol{Y}_{N-1}+C\boldsymbol{Y}_0-\boldsymbol{Y}_1+D_0\boldsymbol{Y}_0=\boldsymbol{F}_0,\quad j=0,\quad \boldsymbol{Y}_0=\boldsymbol{Y}_N. \quad (3.2.10)$$

where $N=n_\theta$. Here for $j=0,\dots N-1$ we used the following notations:

$$\boldsymbol{Y}_j=(y(1,j),y(2,j),\dots,y(n_r,j)),$$
$$\boldsymbol{F}_j=(t_1\hat{f}(1,j),t_2\hat{f}(2,j),\dots,t_{n_r}\hat{f}(n_r,j)),$$
$$C\boldsymbol{Y}_j=\big((2E-t_1\boldsymbol{\Lambda})y(1,j),\dots,(2E-t_{n_r}\boldsymbol{\Lambda})y(n_r,j)\big),$$
$$D_j\boldsymbol{Y}_0=(t_1\hat{c}_{1,j}y(i^*,0),\dots,t_{n_r}\hat{c}_{n_r,j}y(i^*,0)).$$

Moreover,

$$\hat{f}(i,j) = \begin{cases} -f(i,j) & \text{if } 1 \le i \le n_r - 1, \\ -f(i,j) - \frac{r_{pc}}{\rho \hat{s}} g^{(2)} & \text{if } i = n_r. \end{cases}$$

$$\hat{c}(i,j) = \begin{cases} -c(1,j) + \frac{a_1^-}{\rho s_0 \hat{s}} g_j^{(1)} & \text{if } i = 1. \\ -c(i,j) & \text{if } 1 \le i \le n_r - 1, \\ -c(n_r,j) + \frac{a_{n_r}^-}{\rho \hat{s}} g_j^{(3)} & \text{if } i = n_r. \end{cases}$$

and the difference operator $\mathbf{\Lambda}$ is given by the formula:

$$\mathbf{\Lambda} y = \begin{cases} \frac{1}{\rho \hat{s}} \left(\left(\frac{a^-}{s_0} + \frac{a_1}{s_1} \right) y_{1,j} + \frac{a^+}{s_1} y_{2,j} \right) & \text{if } i = 1, \\ \frac{1}{\rho \hat{s}} \left(\frac{a^-}{s_{i-1}} y_{i-1,j} - \left(\frac{a^-}{s_{i-1}} + \frac{a^+}{s_i} \right) y_{i,j} + \frac{a^+}{s_i} y_{i+1,j} \right) & \text{if } 2 \le i \le n_r - 1, \\ -\frac{a^-}{\rho_i \hat{s} s_{i-1}} (y_{n_r,j} - y_{n_r-1,j}) & \text{if } i = n_r, \end{cases}$$

and, finally, E is a unit matrix, $t_i = \rho^2(i) s_\theta / b_i^3$. With these notations C and D_j are matrices of the size $nr \times nr$. The row i of C correspond to the row i of $(2E - t_i \mathbf{\Lambda})$. Note, that matrix C is tridiagonal, which will allow us to use Thomas algorithm for inverting it. Matrix D_j has zeros entries everywhere, but the column i^* is the vector $(t_1 \hat{c}_{1,j}, t_2 \hat{c}_{2,j}, \ldots, t_{n_r} \hat{c}_{n_r,j})$. Thus, where it is convenient and possible, D_j can be treated as a vector. To solve this system we modified the reduction method described in [17] to consider also the additional term with $y(i^*, 0)$.

3.2.1.1 Modified reduction method

Let us describe in details the modified method of reduction for solving the system (3.2.10) as in [17]. The number of points in θ for the method should be a power of 2, $N = 2^n$. In (3.2.10) for $j = 2,\ 4,\ 6,\ \ldots,\ N-2$ let us eliminate the variables $\boldsymbol{Y}_j$ with odd numbers from two neigbouring equations. We will get

$$\begin{aligned} &-\boldsymbol{Y}_{j-2} + C^{(1)} \boldsymbol{Y}_j - \boldsymbol{Y}_{j+2} + D_j^{(1)} \boldsymbol{Y}_0 = \boldsymbol{F}_j^{(1)}, \quad j = 2,\ 4,\ \ldots,\ N-2, \\ &-\boldsymbol{Y}_2 + C^{(1)} \boldsymbol{Y}_0 - \boldsymbol{Y}_2 + D_j^{(1)} \boldsymbol{Y}_0 = \boldsymbol{F}_0^{(1)}, \end{aligned}$$

where

$$C^{(1)} = C^2 - 2E,\ \boldsymbol{F}_j^{(1)} = \boldsymbol{F}_{j-1}^{(0)} + C\boldsymbol{F}_j^{(0)} + \boldsymbol{F}_{j+1}^{(0)},\ D_j^{(1)} = D_{j-1}^{(0)} + CD_j^{(0)} + D_{j+1}^{(0)},$$

$$\boldsymbol{F}_0^{(1)} = \boldsymbol{F}_{N-1}^{(0)} + C\boldsymbol{F}_0^{(0)} + \boldsymbol{F}_1^{(0)},\ D_0^{(1)} = D_{N-1}^{(0)} + CD_0^{(0)} + D_1^{(0)}, \boldsymbol{F}_j^{(0)} = \boldsymbol{F}_j,\ D_j^{(0)} = D_j.$$

Then, the unknowns $\boldsymbol{Y}_j$ with odd numbers can be found from the equations:

$$C^{(0)}\boldsymbol{Y}_j = \boldsymbol{F}_j^{(0)} + \boldsymbol{Y}_{j-1} + \boldsymbol{Y}_{j+1} - D_j^{(0)}\boldsymbol{Y}_0, \qquad j = 1,\ 3,\ 5,\ \ldots,\ N-1, \quad C^{(0)} = C$$

The process of elimination can be continued. After the step l we will get the system of equations for the unknowns $\boldsymbol{Y}_j$ with j being a multiple of 2^l:

$$-\boldsymbol{Y}_{j-2^l} + C^{(l)}\boldsymbol{Y}_j - \boldsymbol{Y}_{j+2^l} + D_j^{(l)}\boldsymbol{Y}_0 = \boldsymbol{F}_j^{(l)}, \quad j = 2^l, 2\cdot 2^l, \ldots, N-2^l,$$
$$-\boldsymbol{Y}_{2^l} + C^{(l)}\boldsymbol{Y}_0 - \boldsymbol{Y}_{2^l} + D_j^{(l)}\boldsymbol{Y}_0 = \boldsymbol{F}_0^{(l)},$$

along with the group of equations

$$C^{(k-1)}\boldsymbol{Y}_j = \boldsymbol{F}_j^{(k-1)} + \boldsymbol{Y}_{j-2^{k-1}} + \boldsymbol{Y}_{j+2^{k-1}} - D_j^{(k-1)}\boldsymbol{Y}_0, \tag{3.2.11}$$
$$j = 2^{k-1}, 3\cdot 2^{k-1}, 5\cdot 2^{k-1}, \ldots, N-2^{k-1}, k = l,\ l-1, \ldots,\ 1,\ C^{(k)} = (C^{(k-1)})^2 - 2E$$

for obtaining rest of the variables. $\boldsymbol{F}_j^{(k)}$ and $D_j^{(k)}$ are defined recurrently for $k = 1, 2, ..., n-1$ as

$$\boldsymbol{F}_j^{(k)} = \boldsymbol{F}_{j-2^{k-1}}^{(k-1)} + C^{(k-1)}\boldsymbol{F}_j^{(k-1)} + \boldsymbol{F}_{j+2^{k-1}}^{(k-1)},\ D_j^{(k)} = D_{j-2^{k-1}}^{(k-1)} + C^{(k-1)}D_j^{(k-1)} + D_{j+2^{k-1}}^{(k-1)},$$
$$j = 2^k, 2\cdot 2^k, 3\cdot 2^k, \ldots, N-2^k, \qquad \boldsymbol{F}_j^{(0)} = \boldsymbol{F}_j, \qquad D_j^{(0)} = D_j, \tag{3.2.12}$$
$$\boldsymbol{F}_0^{(k)} = \boldsymbol{F}_{N-2^{k-1}}^{(k-1)} + C^{(k-1)}\boldsymbol{F}_0^{(k-1)} + \boldsymbol{F}_{2^{k-1}}^{(k-1)},\ D_0^{(k)} = D_{N-2^{k-1}}^{(k-1)} + C^{(k-1)}D_0^{(k-1)} + D_{2^{k-1}}^{(k-1)},$$

For the step $n-1$ we will obtain the system for $\boldsymbol{Y}_0$ and $\boldsymbol{Y}_{2^{n-1}}$ ($\boldsymbol{Y}_N = \boldsymbol{Y}_0$):

$$C^{(n-1)}\boldsymbol{Y}_{2^{n-1}} + (D_{2^{n-1}}^{(n-1)} - 2E)\boldsymbol{Y}_0 = \boldsymbol{F}_{2^{n-1}}^{(n-1)},$$
$$-2\boldsymbol{Y}_{2^{n-1}} + (C^{(n-1)} + D_0^{(n-1)})\boldsymbol{Y} = \boldsymbol{F}_0^{(n-1)}. \tag{3.2.13}$$

By solving this system we will find $\boldsymbol{Y}_0,\ \boldsymbol{Y}_{2^{n-1}}$ and $\boldsymbol{Y}_N = \boldsymbol{Y}_0$. The rest of the unknowns can be found from (3.2.11) as the solutions of the equations:

$$C^{(k-1)}\boldsymbol{Y}_j = \boldsymbol{F}_j^{(k-1)} + \boldsymbol{Y}_{j-2^{k-1}} + \boldsymbol{Y}_{j+2^{k-1}} - D_j^{(k-1)}\boldsymbol{Y}_0,$$
$$j = 2^{k-1}, 3\cdot 2^{k-1}, 5\cdot 2^{k-1}, \ldots, N-2^{k-1}, \quad k = n,\ n-1, \ldots,\ 1.$$

However, before we solve (3.2.13) we would like to use complementary vectors $\boldsymbol{p}_j^{(k)},\ \boldsymbol{q}_j^{(k)}$ and $\boldsymbol{l}_j^{(k)},\ \boldsymbol{m}_j^{(k)}$ connected to $\boldsymbol{F}_j^{(k)}$ and $D_j^{(k)}$ with the following relations

$$\begin{aligned}
&\boldsymbol{F}_j^{(k)} = C^{(k)}\boldsymbol{p}_j^{(k)} + \boldsymbol{q}_j^{(k)},\\
&D_j^{(k)} = C^{(k)}\boldsymbol{l}_j^{(k)} + \boldsymbol{m}_j^{(k)}, \quad j = 0, 2^k, 2\cdot 2^k, 3\cdot 2^k, \ldots, N-2^k.
\end{aligned} \tag{3.2.14}$$

Note that D_j is a matrix which has zero entries everywhere, except of the column i^*. Thus, where convenient D_j is considered to be a vector. We will introduce the way to find $\boldsymbol{p}_j^{(k)},\ \boldsymbol{q}_j^{(k)}$, and $\boldsymbol{l}_j^{(k)},\ \boldsymbol{m}_j^{(k)}$ can be found by following the same procedure. Using the recurrent formulas (3.2.12) we will obtain the relations

$$\begin{aligned}
&C^{(k-1)}\mathbf{S}_j^{(k-1)} = \boldsymbol{q}_j^{(k-1)} + \boldsymbol{p}_{j-2^{k-1}}^{(k-1)} + \boldsymbol{p}_{j+2^{k-1}}^{(k-1)},\\
&\boldsymbol{p}_j^{(k)} = \boldsymbol{p}_j^{(k-1)} + \mathbf{S}_j^{(k-1)},\\
&\boldsymbol{q}_j^{(k)} = 2\boldsymbol{p}_j^{(k)} + \boldsymbol{q}_{j-2^{k-1}}^{(k-1)} + \boldsymbol{q}_{j+2^{k-1}}^{(k-1)},\\
&j = 2^k,\ 2\cdot 2^k,\ ,3\cdot 2^k,\ \ldots,\ N-2^k, \quad k = 1,\ 2,\ \ldots,\ n-1,\\
&\boldsymbol{q}_j^{(0)} = \boldsymbol{F}_j,\ \boldsymbol{p}_j^{(0)} = 0,\ j = 1,\ 2,\ ,\ \ldots,\ N-1,
\end{aligned} \tag{3.2.15}$$

from which we can find $\boldsymbol{p}_j^{(k)},\ \boldsymbol{q}_j^{(k)}$ for $j \neq 0$ and formulas

$$\begin{aligned}
&C^{(k-1)}\mathbf{S}_0^{(k-1)} = \boldsymbol{q}_0^{(k-1)} + \boldsymbol{p}_{2^{k-1}}^{(k-1)} + \boldsymbol{p}_{N-2^{k-1}}^{(k-1)},\\
&\boldsymbol{p}_0^{(k)} = \boldsymbol{p}_0^{(k-1)} + \mathbf{S}_0^{(k-1)},\\
&\boldsymbol{q}_0^{(k)} = \boldsymbol{p}_0^{(k)} + \boldsymbol{q}_{2^{k-1}}^{(k-1)} + \boldsymbol{q}_{N-2^{k-1}}^{(k-1)}, \quad k = 1,\ 2,\ \ldots,\ n-1,\\
&\boldsymbol{q}_0^{(0)} = \boldsymbol{F}_0,\ \boldsymbol{p}_0^{(0)} = 0,
\end{aligned} \tag{3.2.16}$$

for finding $\boldsymbol{p}_0^{(k)}$, and $\boldsymbol{q}_0^{(k)}$. Now we can solve system (3.2.13). From (3.2.15) and (3.2.16) for $k = n-1$ we can obtain

$$\begin{aligned}
\boldsymbol{q}_{2^{n-1}}^{(n-1)} &= 2\boldsymbol{p}_{2^{n-1}}^{(n-1)} + \boldsymbol{q}_{2^{n-2}}^{(n-2)} + \boldsymbol{q}_{3\cdot 2^{n-1}}^{(n-2)},\\
\boldsymbol{q}_0^{(n-1)} &= 2\boldsymbol{p}_0^{(n-1)} + \boldsymbol{q}_{2^{n-2}}^{(n-2)} + \boldsymbol{q}_{3\cdot 2^{n-1}}^{(n-2)},
\end{aligned}$$

from which we can find

$$\boldsymbol{q}_0^{(n-1)} - \boldsymbol{q}_{2^{n-1}}^{(n-1)} = 2(\boldsymbol{p}_0^{(n-1)} - \boldsymbol{p}_{2^{n-1}}^{(n-1)}). \tag{3.2.17}$$

The analogous relation can be obtained for $\boldsymbol{l}_j^{(k)}$ and $\boldsymbol{m}_j^{(k)}$

$$\boldsymbol{m}_0^{(n-1)} - \boldsymbol{m}_{2^{n-1}}^{(n-1)} = 2(\boldsymbol{l}_0^{(n-1)} - \boldsymbol{l}_{2^{n-1}}^{(n-1)}). \tag{3.2.18}$$

Let us subtract the first equation of (3.2.13) from the second one and apply the formulas (3.2.17),(3.2.18) to obtain

$$(C^{(n-1)}+2E)(\boldsymbol{Y}_0-\boldsymbol{Y}_{2^{n-1}})+\left(D_0^{(n-1)}-D_{2^{n-1}}^{(n-1)}\right)\boldsymbol{Y}_0=$$
$$\left[C^{(n-2)}\right]^2\left(\boldsymbol{Y}_0-\boldsymbol{Y}_{2^{n-1}}+\left(\boldsymbol{l}_0^{(n-1)}-\boldsymbol{l}_{2^{n-1}}^{(n-1)}\right)\boldsymbol{Y}_0\right)=\left[C^{(n-2)}\right]^2\left(\boldsymbol{l}_0^{(n-1)}-\boldsymbol{l}_{2^{n-1}}^{(n-1)}\right).$$

Assuming that $C^{(n-2)}$ is not singular, we can obtain the relation

$$\boldsymbol{Y}_{2^{n-1}}=\left[E+\boldsymbol{l}_0^{(n-1)}-\boldsymbol{l}_{2^{n-1}}^{(n-1)}\right]\boldsymbol{Y}_0-\boldsymbol{p}_0^{(n-1)}+\boldsymbol{p}_{2^{n-1}}^{(n-1)}. \tag{3.2.19}$$

Therefore, using (3.2.19), from the second equation of (3.2.13) we get

$$(C^{(n-1)}-2E)\left(\boldsymbol{Y}_0-\boldsymbol{l}_0^{(n-1)}\boldsymbol{Y}_0\right)+2\boldsymbol{l}_{2^{n-1}}^{(n-1)}\boldsymbol{Y}_0=\boldsymbol{F}_{2^{n-1}}^{(n-1)}-2\boldsymbol{p}_0^{(n-1)}+2\boldsymbol{p}_{2^{n-1}}^{(n-1)}=$$
$$=(C^{(n-1)}-2E)\boldsymbol{p}_0^{(n-1)}+\boldsymbol{q}_{2^{n-1}}^{(n-1)}+2\boldsymbol{p}_{2^{n-1}}^{(n-1)}$$

We denote $B=(C^{(n-1)}-2E)$. This matrix can be easily inverted, thus, we can find $\boldsymbol{Y}_0$ from the relations

$$\begin{aligned}
&B\mathbf{s_1}=2\boldsymbol{l}_{2^{n-1}}^{(n-1)},\\
&B\mathbf{s_2}=\boldsymbol{q}_{2^{n-1}}^{(n-1)}+2\boldsymbol{q}_{2^{n-1}}^{(n-1)},\\
&(E+\boldsymbol{l}_0^{(n-1)}+\mathbf{s_1})\boldsymbol{Y}_0=\boldsymbol{p}_0^{(n-1)}+\mathbf{s_2}.
\end{aligned} \tag{3.2.20}$$

where $\mathbf{s_1}$ and $\mathbf{s_2}$ are the vectors in first two equations and matrices which have zero entries everywhere except the column i^* in the last one. We can find $\boldsymbol{Y}_{2^{n-1}}$ from (3.2.19) and the rest of the variables can be found from the formulas

$$\begin{aligned}
&\boldsymbol{Y}_N=\boldsymbol{Y}_0,\\
&C^{(k-1)}\mathbf{t}_j^{(k-1)}=\boldsymbol{q}_j^{(k-1)}+\boldsymbol{Y}_{j-2^{k-1}}+\boldsymbol{Y}_{j+2^{k-1}}-\boldsymbol{m}_j^{(k-1)}\boldsymbol{Y}_0,\\
&\boldsymbol{Y}_0=\boldsymbol{p}_j^{(k-1)}+\mathbf{t_j}^{(k-1)}-\boldsymbol{l}_j^{(k-1)}\boldsymbol{Y}_0,\\
&j=2^{k-1},\ 3\cdot 2^{k-1},\ 5\cdot 2^{k-1},\ \ldots,\ N-2^{k-1},\\
&k=n-1,\ n-2,\ \ldots,\ 1.
\end{aligned} \tag{3.2.21}$$

Therefore, the equations (3.2.15)-(3.2.16), (3.2.19)-(3.2.21) describe the modified method of reduction for solving the system (3.2.10). For inverting the matrices $C^{(n-1)}$ and B we

use the factorizations proposed in [17]

$$C^{(k-1)} = \prod_{l=1}^{2^{k-1}} C_{l,k-1}, \qquad C_{l,k-1} = C - 2\cos\frac{(2l-1)\pi}{2^k}E, \tag{3.2.22}$$

$$B = \left[\prod_{k=1}^{n-2}\prod_{l=1}^{2^{k-1}} C_{l,k-1}\right]^2 (C-2E)(C+2E). \tag{3.2.23}$$

Note that for given tridiagonal C, all the matrices $C_{l,k-1}$ are tridiagonal as well. Thus, for inverting them we use tridiagonal matrix algorithm (TDMA), also known as Thomas algorithm (can be found in [17]).

The equations were coded in Python and the results were obtained as shown in § 3.3.

3.2.2 Case of multiple holes

The equations for the regularized pressure in case when we have N_h iridotomies are derived in § 3.1.2:

$$\boldsymbol{\nabla}\cdot\left(h^3\boldsymbol{\nabla}p_{\mathsf{reg}}\right) = -\sum_{i=1}^{N_h}\frac{6\mu Q_i}{\pi r_i h_i^3}\frac{\partial h^3}{\partial r_i} + 12\mu\Big(\frac{h}{2}\boldsymbol{\nabla}\cdot v_r - v_r\cdot h' + v_z\Big) \tag{3.2.24}$$

$$Q_i = \frac{\pi a_i^4}{8S\mu + 3\pi\mu a_i}\, p_{\mathsf{reg}}|_i + \sum_{j=1, i\neq j}^{N_h}\frac{6a_i^4 Q_j}{h_j^3(8S+3\pi a_i)}\ln\frac{d_{ij}}{a_j} \qquad \text{at the point } i,\ i=1,...,N_h\ , \tag{3.2.25}$$

$$\frac{\partial p_{\mathsf{reg}}}{\partial r} = \frac{6\mu F}{\pi r_{pc}h^3} + \frac{6\mu v_r}{h^2} - \sum_{1}^{N_h}\frac{6\mu Q_i}{\pi r_i h_i^3}\frac{\partial r_i}{\partial r} \qquad \text{flux boundary condition at } r = r_{pc}, \tag{3.2.26}$$

$$p_{\mathsf{reg}} = -\sum_{1}^{N_h}\frac{6\mu Q_i}{\pi h_i^3}\ln\frac{r_i}{a_i} \qquad \text{at the pupil } r = r_p, \tag{3.2.27}$$

where r_i is given by relations (3.1.11), $h_i = h(d_i)$ - height of the domain in the point of the hole.

The idea of solving the equation is to make an iterative process. Denote $Q = (Q_1, \ldots, Q_{N_h})$ - vector of fluxes through the holes. By knowing Q we can find p_{reg} and vice versa. We start from initial configuration for $Q^{(0)} = 0$. With the given $Q^{(0)}$ we can find $p_{\mathsf{reg}}^{(0)}$ by

solving the equation (3.2.24) with the boundary conditions (3.2.26)-(3.2.27). Then , from the condition (3.2.25) we find $Q^{(1)}$. Thus, step k consists of the following procedure: for given $Q^{(k)}$ we solve the system to find $p_{\mathsf{reg}}^{(k)}$, while not reaching given tolerance $\epsilon : \|Q^{(k)} - Q^{(k-1)}\| < \epsilon$. For every k the problem can be solved using finite difference method. The discretization is similar to the case one hole. The grid ω, step s, average step $\hat{s}$ and grid function ρ are defined in the same way as in § 3.2.1. Then, the equation (3.2.24) we will write as

$$\frac{1}{\rho\hat{s}}\left(\frac{a_i^-}{s_{i-1}}y_{i-1,j} - \left(\frac{a_i^-}{s_{i-1}} + \frac{a_i^+}{s_i}\right)y_{i,j} + \frac{a_i^+}{s_i}y_{i+1,j}\right) + \frac{b_i}{\rho^2}\,\frac{y_{i,j-1} - 2y_{i,j} + y_{i,j+1}}{s_\theta^2} = f_{i,j},$$
$$1 \le i \le n_r - 1,\ 0 \le j \le n_\theta - 1, \quad (3.2.28)$$

where a_i^+, a_i^-, b_i are defined in the same way as before, $f(r,\theta) = -\sum_{i=1}^{N_h} \frac{6\mu Q_i^{(k)}}{\pi r_i h_i^3}\frac{\partial h^3}{\partial r_i} + 12\mu\Big(\frac{h}{2}\boldsymbol{\nabla}\cdot v_r - v_r\cdot h' + v_z\Big)$, $f_{i,j} = f(r_i,\theta_j)$. The boundary conditions (3.2.26)-(3.2.27) can be written as

$$y_{0,j} = -\sum_1^{N_h}\frac{3\mu Q_i}{\pi h_i^3}\ln\left(\frac{r_p^2 + d_{\mathsf{hole}}^2 - 2d_{\mathsf{hole}}r_p\cos\theta_j}{a_{\mathsf{hole}}^2}\right), \quad 0 \le j \le n_\theta - 1, \quad i = 0 \quad (3.2.29)$$

$$-\frac{a_i^-}{\rho\hat{s}s_{n_r-1}}(y_{n_r,j} - y_{n_r-1,j}) + \frac{b_i}{\rho^2}\cdot\left(\frac{y_{n_r,j-1} - 2y_{n_r,j} + y_{n_r,j+1}}{s_\theta^2}\right) =$$
$$= f_{n_r,j} - \frac{r}{\rho\hat{s}}\left(-\frac{6\mu F}{\pi r_{pc}} + \sum_1^{N_h}\frac{6\mu h^3 Q_i}{\pi r_i h_i^3}\frac{\partial r_i}{\partial r}\right) \quad 0 \le j \le n_\theta - 1, \quad i = n_r \quad (3.2.30)$$

where (3.2.27) is discretized using the "ghost point" method. Therefore, for each iterative step k with given $Q^{(k)}$ we will find corresponding p_{reg} by solving the system of discretized equations (3.2.28) - (3.2.30). In order to speed up the computational process the method called "complete reduction" was used for solving the linear system. The method is described in [17]. It can be also done with the method from § 3.2.1.1, with D_j being a zero matrix. Therefore, we will not describe it here. The equations were coded and the results are shown in § 3.3

3.3 Results

In this section we will present and analyse the results obtained for the iridotomy model described above. All the simulations were done in Python using the packages numpy,

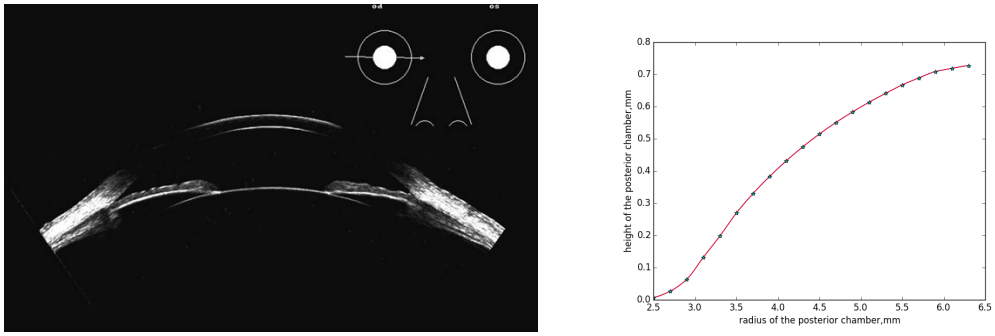

(A) Ultrasound image of the anterior part of the human eye

(B) Interpolated height of the posterior chamber

FIGURE 3.1: The shape of the posterior chamber

scipy and ,matplotlib packages. The resolution in the θ component was taken in the range $2^{10} - 2^{12}$, and in range $400 - 600$ in r component. First we will introduce the function h, which we used for all the simulations. Then we will proceed to the results for two different scenarios: the flow due to the aqueous production (§ 3.3.2) and the flow due to miosis (§ 3.3.3). Then, we will compare the obtained results in § 3.3.4.

3.3.1 Geometry

For all the simulations we used a realistic geometry taken from an ultrasound picture of the domain (fig. 3.1a). Since the posterior chamber is located behind the iris that is not a transparent tissue other optically based techniques, such as OCT (optical coherence tomography) cannot be used to visualise the posterior chamber. In order to obtain high resolution image very high frequency ultrasound scans should be used. Since such an instrument was not available in the working group asit is not normally employed in the clinical practice, we analysed an image freely available on the Internet. We proceeded by measuring the height of the posterior chamber for left part of the image in MatCad for 20 points. Then, we used the Python function PchipInterpolator from the scipy.interpolate package, which for given arrays x and y performs a monotone smooth interpolation. Therefore, we obtained an approximate height of the domain (which we consider to be axisymmetric) and it is shown in a figure 3.1b. The ultrasound scan resolution is not good enough to resolve the tiny passage between the lens and the iris. Thus, for the height of the iris-lens channel we assumed the value of ~ 7 μm ([6])

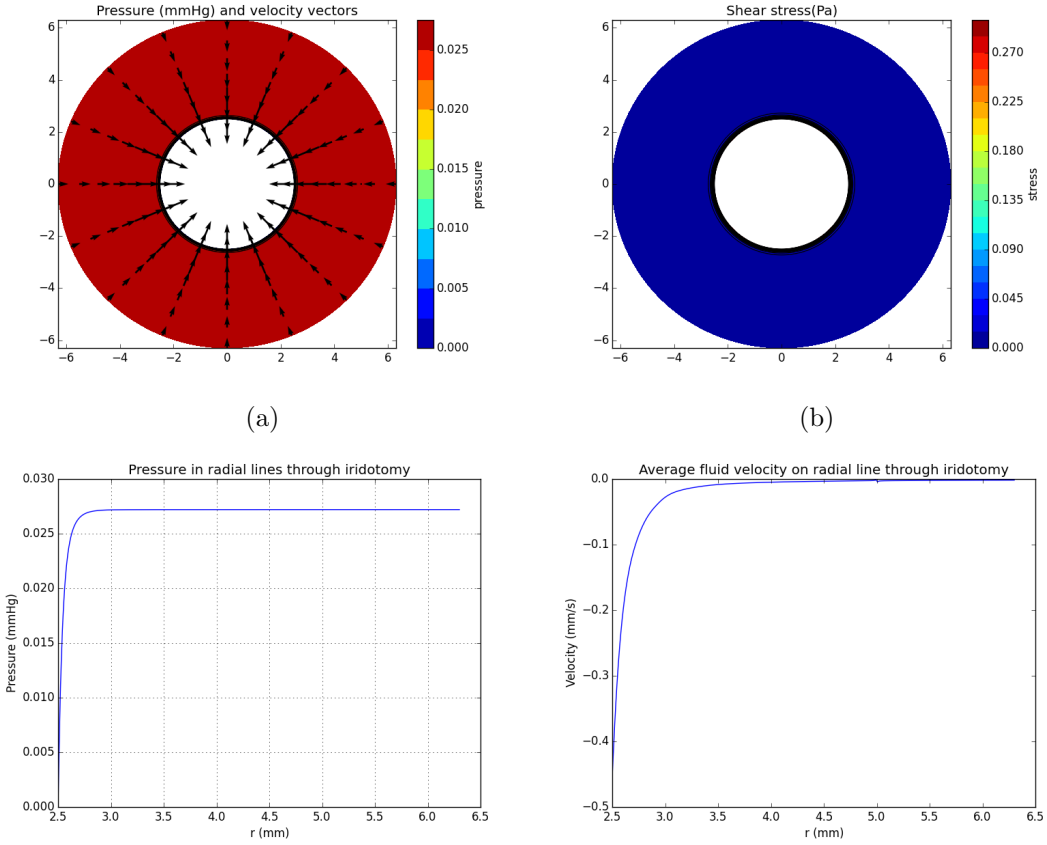

FIGURE 3.2: The pressure, velocity (a,c,d) and wall shear stress on the iris (b) without the iridotomy

3.3.2 Flow due to aqueous production

We are interested in the pressure distribution, velocity profile and flux through the iridotomy. Figures 3.2-3.3 represent the results for the flow without the iridotomy (fig. 3.2), and with the iridotomy of radii 50μm and 100 μm (fig. 3.3). The hole is located along the positive x-axis, at a distance of 5 mm from the center of the pupil. Figure 3.2 (a) and (b) represents the view on the domain from the top, the inner circle represents the pupil, the outer one the boundary of the posterior chamber. In (a) the color-bar represents the pressure distribution and the arrows are the vertically averaged velocity vectors. In (b) the color-bar describes the wall shear stress on the domain. In figures (c) and (d) the x-axis is the radial coordinate r spanning the region from the radius of the pupil (left) to the outer boundary of the posterior chamber (right). Note, that the pressure along the radial line through the iridotomy and the wall shear stress look very similar to each other for different sizes of iridotomy, just differing in magnitude.

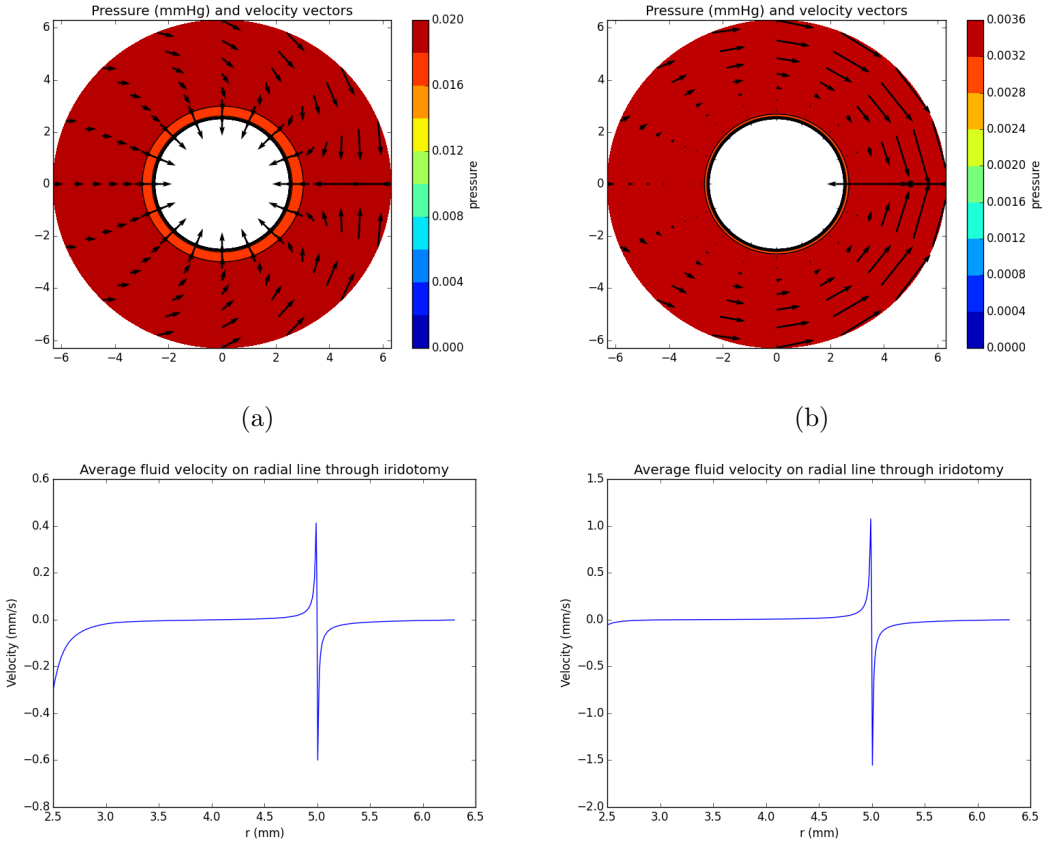

FIGURE 3.3: Pressure distribution and average velocity vectors (a,b) and the average velocity on the radial line through iridotomy (c,d). Radius of iridotomy in (a,c) is 50μm, in (b,d) - 100μm

Therefore, in the figure 3.3 we plotted only the pressure distribution and average velocity vectors (a,b) and the average velocity distribution along the radial line through iridotomy (c,d).

From these figures we can observe that the pressure distribution along the radial line is almost constant everywhere and it is decreasing rapidly close to the pupil. This is due to the fact that the channel iris-lens is very thin compared to the rest of the domain. Note that the maximum pressure in the posterior chamber decreases with increasing size of the iridotomy; however, it is relatively small even for small iridotomies. The wall shear stress on the iris is also decreasing with the increasing size of the hole. We observe that the shear stress is highest around the pupil and, in case of bigger holes, around the iridotomy as well. The velocity profile increases in magnitude towards the pupil and has a discontinuity across the point of the iridotomy. The table 3.1 shows the percentage of the flux through the hole and the relative error in terms of flux conservation for different

Radius of the iridotomy a_{hole}	Flux through the iridotomy Q_{hole}	Relative error
10 μm	0.09%	0.35%
50 μm	33.72%	0.33%
100 μm	87.58%	0.29%

TABLE 3.1: The percent of the flux through the iridotomy for different sizes of the hole

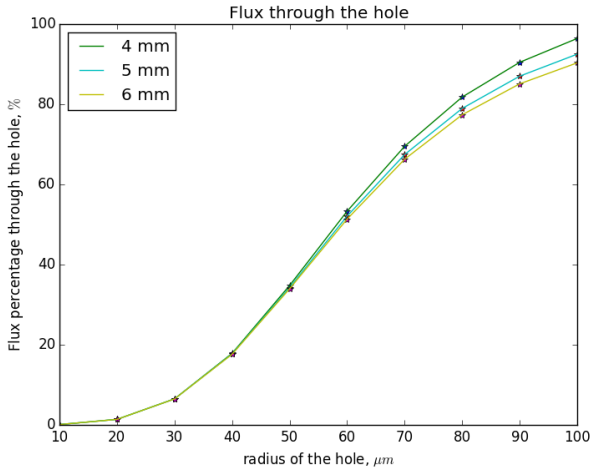

FIGURE 3.4: Flux percentage through the iridotomy out of the total incoming flux depending on different radii of iridotomy for different places of the hole

sizes of the iridotomy. The iridotomy is placed at the distance of 5 mm from the center of the pupil. The relative error here is a percentage of deviation of the total outflow from the inflow, error= $(Q_{\text{hole}} + Q_{\text{pupil}} - F)/F \cdot 100\%$, where Q_{pupil} is the flux going out of the pupil.

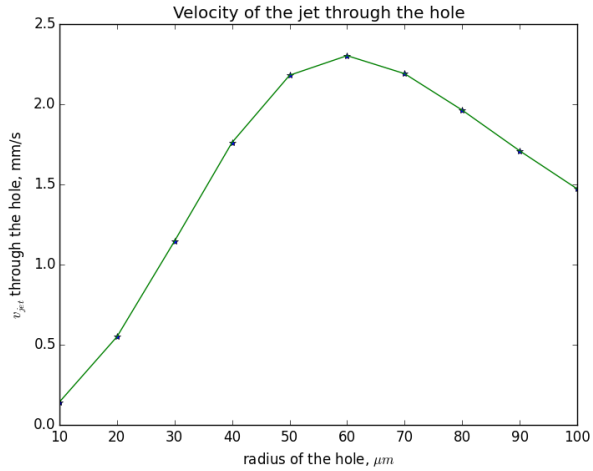

FIGURE 3.5: Velocity of the jet through the iridotomy vs size of iridotomy

In figure 3.4 we plotted the percentage of flux through the hole out of the total flux produced by ciliary body depending on the size of the iridotomy. The green line corresponds to the case in which the iridotomy is placed at a distance 4 mm from the center of the pupil, the blue line - 5 mm and the yellow one - 6 mm. This plot suggests that the place of the iridotomy is not affecting much the flux through the iridotomy, whereas with the variation of the radius of the hole the flux varies from 0 to approximately 100 %.

Another possible concern one might have in case of iridotomy is the magnitude of the velocity of the jet from the iridotomy. We are interested in it, since high velocities might cause the detachment of endothelium cells from the cornea (the inner boundary of the anterior chamber). This was postulated by Kaji (2003) [18]. The figure 3.5 shows the velocity of the jet through the hole for different sizes of the hole. We calculated it as a flux through the iridotomy divided by the area of the iridotomy $U = Q_{\mathsf{hole}}/\pi a_{\mathsf{hole}}^2$. This curve has a maximum of 2.3 mm/s in correspondence of the radius 60μm. However, even for the maximum, the velocity is still very small. The value of Reynolds number corresponding to the jet is $Ua_{\mathsf{hole}}/\nu \approx 0.37$. This is extremely small and thus it is non conceivable that the jet might change significantly the wall shear stress on the cornea.

Pupillary block.

Another condition we are interested in is a complete pupillary block. If this happens the iridotomy needs to be performed, to avoid abnormal growth that might cause a closed-angle glaucoma. Thus, we put in our model the flux coming out of the pupil to be zero. This will modify the boundary condition at the pupil, however the methods for the solution will not change. The results for the radius of the iridotomy 50μm are shown on the figure 3.6. For this case we are interested in the maximum of the pressure depending on the size of the iridotomy. The results show that for very small iridotomy size ($\sim 10\mu$m) the pressure growth is almost 30mmHg. By the increasing of the iridotomy size, the maximum pressure decreases very rapidly(fig. 3.7). Indeed, for an iridotomy with a radius of 25μm the maximum pressure drop becomes less then 1mmHg, and for one with radius 50μm it is less then 0.1mmHg. Therefore, it is essential in case of pupillary block to have an iridotomy with a radius larger then 50μm to normalize the pressure.

Multiple holes The case of multiple iridotomies is not very common in ophthalmology. However, there are some cases when it is performed. In figures 3.8 - 3.10 we show the results for the case of multiple iridotomies. Figure 3.8 represents case of 2 holes with radii 40μm and 50μm. In this case the iridotomies are pleced in front of each other at

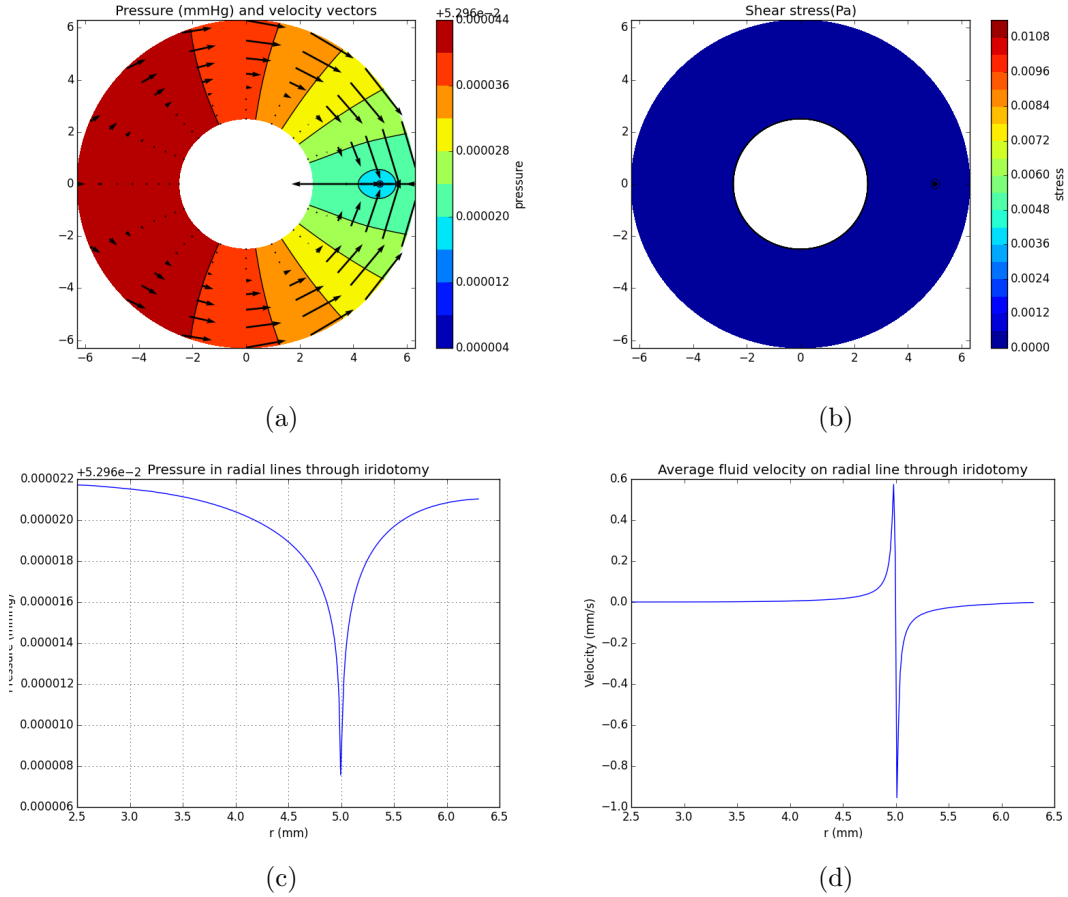

FIGURE 3.6: The pressure, velocity (a,c,d) and wall shear stress on the iris (b) in the case of pupillary block with iridotomy of radius 50μm

opposite sides of the pupil. The fluxes through the holes in this case are 12.43% and 29.57% out of the total incoming flux. In figure 3.9 the result for 3 holes is shown with radii 40, 45, 40μm and placed symmetrically in the domain. The fluxes out of the holes are 12.1%, 19.15%, 12.1% respectively. And finally, the figure 3.10 represents the case of 4 holes with radii 40μm each and placed symmetrically on the eye. The flux percentage out of each iridotomy in this case is 11.56%.

3.3.3 Flow due to miosis

For the case of miosis the flow is more intense due to the imposed velocity on the iris. Let us denote with r_c the radius of the pupil after the contraction, $r_c < r_p$. We recall that we use here the quasi steady approach and solve the problem in the fixed domain coinciding with the initial shape of the posterior chamber. However, we impose a velocity distribution along the iris that depends on the final configuration of the iris at the end of

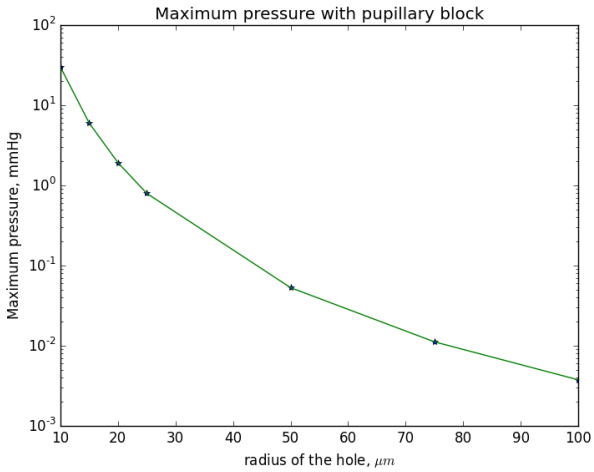

FIGURE 3.7: Maximum pressure in case of pupillary block depending on the size of the iridotomy, the place of the iridotomy is on the distance 5mm from the center of the pupil

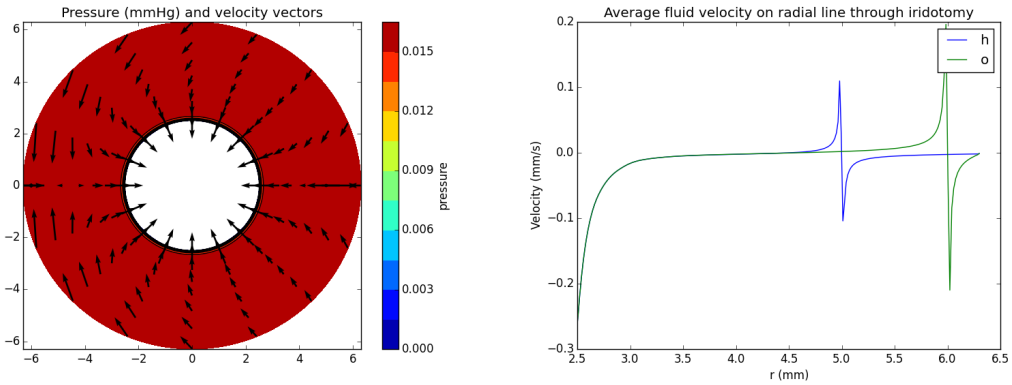

(a) (b)

FIGURE 3.8: 2 holes h and o placed in $(5\text{mm}, 0°)$, $(6\text{mm}, 180°)$ in polar coordinates, with radii 40μm and 50μm respectively. (a) represents pressure distribution and average velocity vectors, in (c) - blue line the average velocity on the radial line through the hole h, the green line - through the hole o.

the pupil contraction. Unfortunately, we do not know exactly how the iris moves during contraction, and a better analysis could be done if more clinical data were available. However, we will make some assumptions that seem to be physically reasonable in order to determine a suitable velocity profile for the iris. Let v_r be the velocity in radial direction, and v_z - vertical velocity. We suppose that the iris on the posterior chamber is not moving, $\mathbf{v}(r_{pc}) = 0$, and from r_p to r_c the iris is moving horizontally, thus $v_z(r_p) = 0$. We put maximum velocity in the radial direction to be $v_{r,max} = (r_p - r_c)/T$ and v_r to be a linear function, $v_r = -\frac{r_p - r_c}{T} \cdot \frac{r - r_{pc}}{r_p - r_{pc}}$ (fig.3.12a). For v_z we choose the function which has its maximum $v_{z,max}$ such that the domain remains concave, and put it to satisfy the

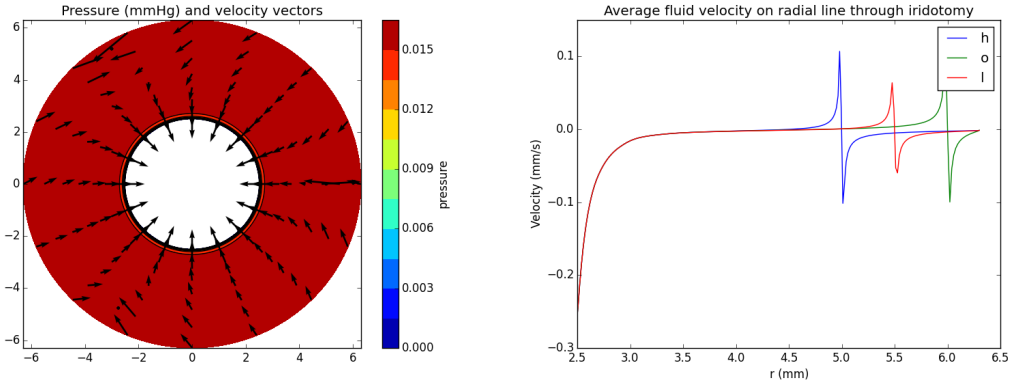

(a) (b)

FIGURE 3.9: 3 holes h,o,l placed in the polar coordinates $(5\text{mm}, 0°)$, $(6\text{mm}, 120°)$, $(5.5\text{mm}, 240°)$ with radii 40, 45, 40μm respectively. (b) shows pressure distribution and average velocity vectors, in (d) blue line is the velocity along the radial line through hole h, red line - through hole l, green one - through hole o.

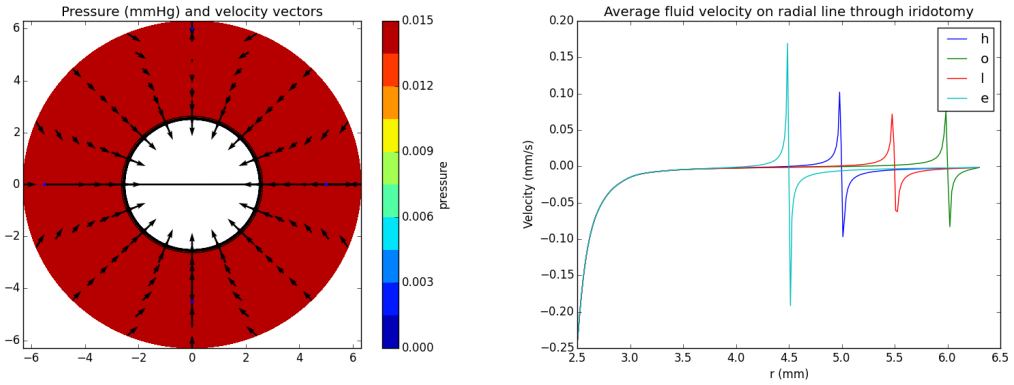

(a) (b)

FIGURE 3.10: 4 holes h,o,l,e placed in the polar coordinates $(5\text{mm}, 0°)$, $(6\text{mm}, 90°)$, $(5.5\text{mm}, 180°)$, $(4.5\text{mm}, 270°)$ all with radius 40μm. (b) shows pressure distribution and average velocity vectors, in (d) blue line is the velocity along the radial line through hole h, red line - through hole l, green one - through hole o, light blue - through the hole e

mentioned assumptions: $v_z = -\frac{v_{z,max}}{T} \sin \frac{\pi(r-r_p)}{r_{pc}-r_p}$ (fig. 3.12b). We will introduce here the results for different sizes of the holes and for different r_c (different imposed velocities).

In the case of miosis we calculate the total incoming flux as sum of the fluxes caused by aqueous production and moving of the iris $Q_{\text{tot}} = F + Q_{\text{wall}}$. Thus we will calculate the percentage of the flux through the iridotomy as $Q_{\text{hole}}/Q_{\text{tot}} \cdot 100\%$. On the figure 3.13 the result for radius of contraction $r_c = 1.5$mm and radius of iridotomy 100μm is shown. The flux percentage through the iridotomy in this case is 85%. On the figure 3.14 we show the result for $r_c = 1$mm and iridotomy size $a_{\text{hole}} = 50\mu$m. We observe that

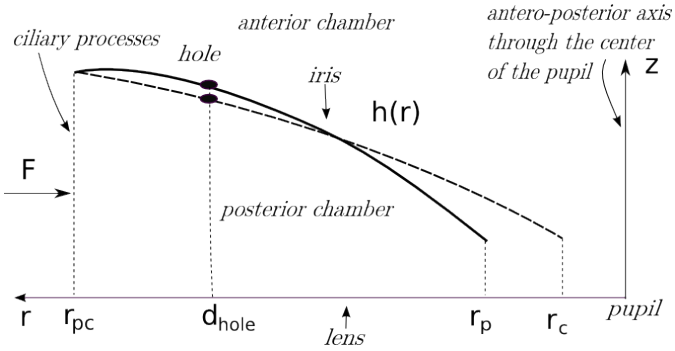

FIGURE 3.11: Vertical cross section of the axisymmetric domain in case of miosis

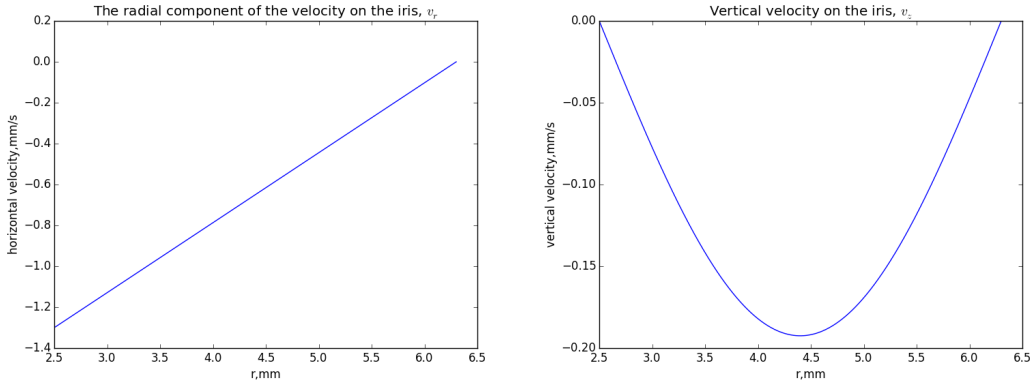

(a) (b)

FIGURE 3.12: The radial and vertical velocities imposed on the iris ($r_c = 1.21$mm)

the pressure is negative and the fluid goes into the posterior chamber both through the iridotomy and the pupil. The flux through the iridotomy in this case is 36%. The figure 3.15a represents the comparison plot for different radius of the contraction $r_c = 1,\ 1.5,\ 2$ mm depending on radius of the iridotomy a_{hole}. The green line denotes the radius of the contraction 1 mm from the center of the pupil, the yellow line - 2 mm and the light blue one - 1.5 mm. This plot suggests that the radius of the contraction of the domain is not affecting the flux percentage out of the total flux, whereas with the variation of the radius of the hole the flux varies roughly from 0 to 100 %. This is similar to what we observe in the case of the steady production/drainage flow. The plot 3.15b shows the flux through the hole and the flux through the pupil for different r_c (which influences the velocity imposed on the iris). We observe that the fluxes become negative for $r_c < 1.2$ mm, meaning that for such cases aqueous humor enters the posterior chamber through the pupil and the iridotomy.

As in the case of aqueous production, we want to observe the velocity of the jet through the hole 3.16. The curve is very similar to the one in figure 3.5, however, the magnitude

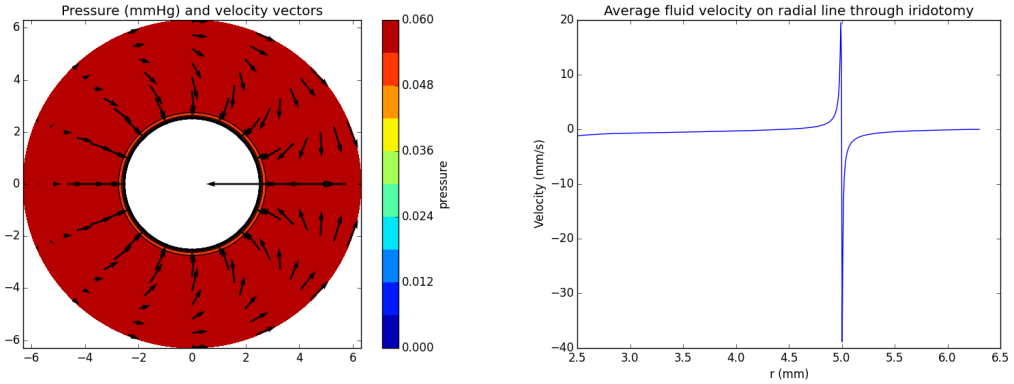

(a) (b)

FIGURE 3.13: Pressure distribution and average velocity vectors (a) and average velocity on the radial line through iridotomy (b) during miosis with contraction radius $r_c = 1.5$mm and iridotomy with radius $a_{\text{hole}} = 100\mu$m

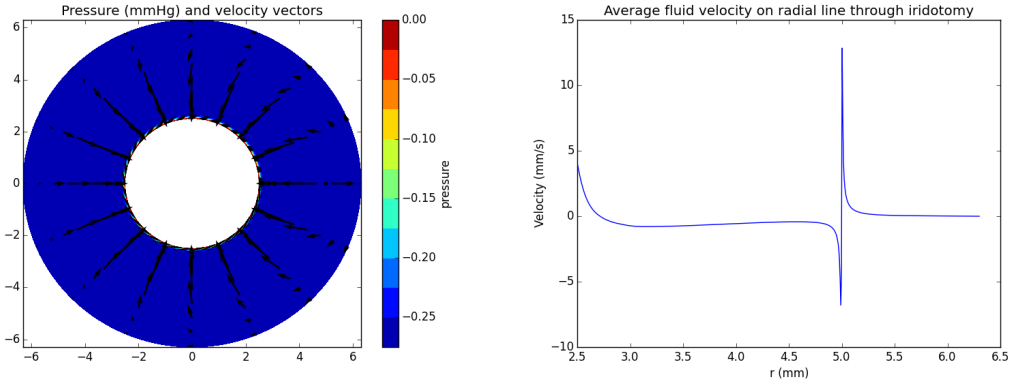

(a) (b)

FIGURE 3.14: Pressure distribution and average velocity vectors (a) and average velocity on the radial line through iridotomy (b) during miosis with contraction radius $r_c = 1$mm and iridotomy with radius $a_{\text{hole}} = 50\mu$m

of the velocity is different. In the case of miosis the maximum magnitude is almost 40 times bigger than in the case of the flow due to aqueous production only, and the Reynolds number can reach a value of ≈ 10. Thus, in this case these can be a variation of wall shear stress on the cornea in the region opposite of iridotomy. The feasibility of such an assumption should be verified modelling the jet behavior in the anterior chamber. This is beyond the scope of this thesis work, but it is an endeavour that will deserve future attention.

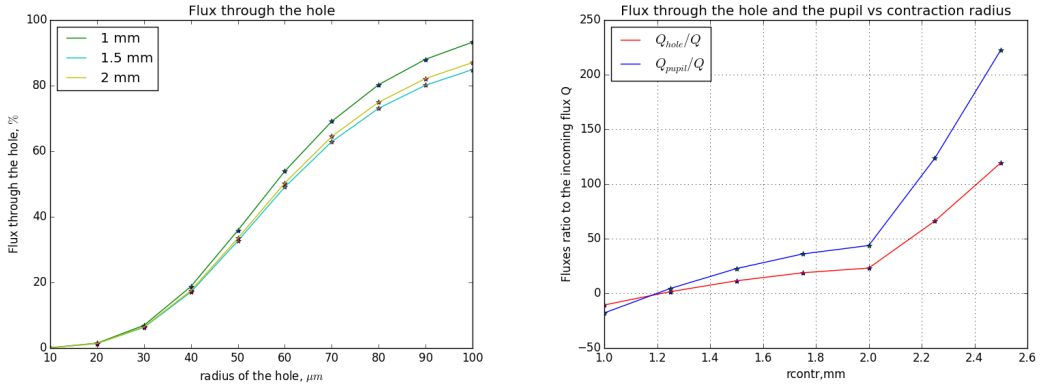

(a) (b)

FIGURE 3.15: (a) flux percentage through the iridotomy out of the total flux Q_{tot} depending on different radii of iridotomy $a_{\text{hole}}$for different radii of the contraction $r_c = 1,\ 1.5,\ 2$mm. (b) Ratio of flux through the hole (red line) and the flux through the pupil (blue) to the incoming flux F, $a_{\text{hole}} = 5\mu$m

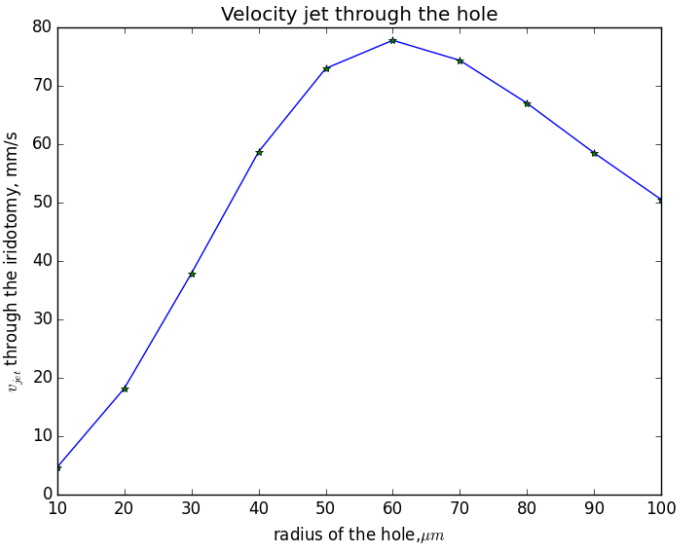

FIGURE 3.16: Velocity of the jet through the iridotomy vs size of iridotomy

3.3.4 Conclusions

From the results in previous section we can make the following conclusions.

- The iridotomy should be at least 40 microns to get a significant impact on the flow. For the small iridotomies (rad. 10μm) the flux through the hole is very small with respect to the total flux. For iridotomies with a radius of $80 - 100\mu$m, almost all the flux goes out of the hole.

- The size of the iridotomy has a big impact on the flux through the iridotomy, whereas the location of the hole has not.
- In the case of pupillary block small iridotomies induce extremely high intraoccular pressures. Thus, for normalizing the pressure in this case one needs the iridotomy of radius at least 50μm.
- During the flow with miosis and the flow due to the aqueous production the percentage of the flux through the iridotomy is very similar for the same sizes of the hole.
- In case of miosis the percentage of the flux through the hole doesn't differ much with various velocities imposed on the iris.
- During miosis the velocity of the jet through the hole is almost 40 times bigger than during the normal case. This is the situation that one has to avoid to prevent cells detachment from cornea.
- The velocity imposed on the iris is very roughly approximated, thus for a better model we need more clinical data, preferably medical images of the posterior chamber before and after pupil contraction.

Chapter 4

Hole-ICL Model

4.1 Mathematical model and assumptions

We are interested in modelling the aqueous flow in the case of implanted Hole-ICL into the posterior chamber of the eye. In the figure 4.1b the cross section of the eye with Hole-ICL is shown. For simplicity we consider axisymmetric domain. For the first model of the problem we assume that the lens is a axisymmetric surface of radius r_l, with a

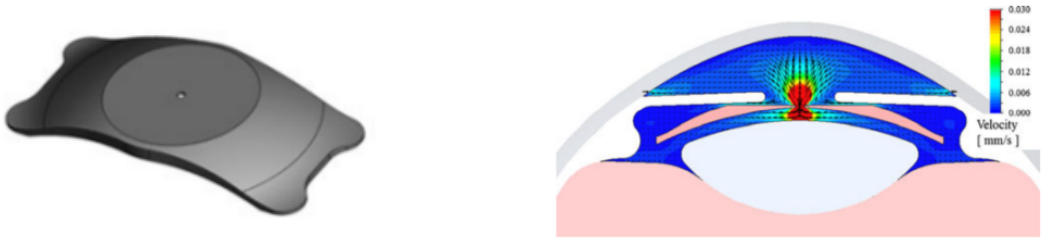

(a) (b)

FIGURE 4.1: The Hole-ICL (a) and the velocity profile with Hole-ICL implanted into the posterior chamber (b), Kawamorita et al. [1]

small hole of radius r_0 in the center. Since the hole is in the center of the lens and both the geometry of the lens and of the posterior chamber are axisymmetric we can consider the flow to be axisymmetric as well. We split the domain of the posterior chamber into three regions with heights $h_i,\ i = 1, 2, 3$ (as it is shown in figure 4.2). Let us define region 1 to be the area without the Hole-ICL, region 2 is the domain between the Hole-ICL and the natural lens, and region 3 is the one between the Hole-ICL and the iris. For every region we want to apply lubrication theory in order to simplify the Navier-Stokes

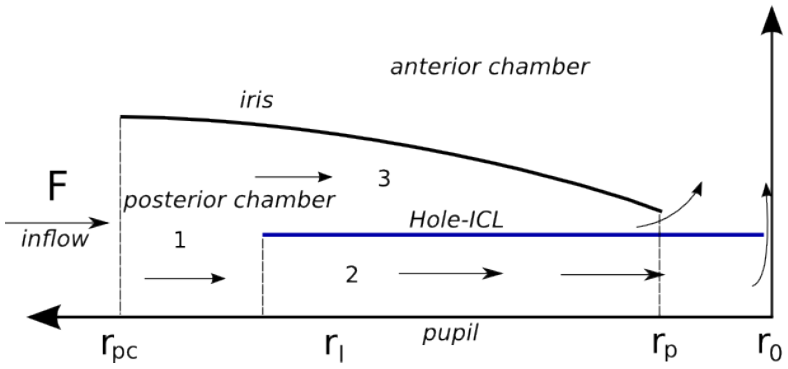

FIGURE 4.2: The vertical cross section of an axisymmetric domain

equations. Indeed, according to the table 4.1 each region can be considered long and thin and, as we did in § 2.2.3 we can drop the terms of order ϵ^2, $\epsilon^2 Re$ compared to order 1 terms in the equations (2.2.1)-(2.2.4). Therefore, for each domain we write the equation for the pressure p_i, $i = 1, 2, 3$ using lubrication theory as in § 2.2.3,

$$\frac{d}{dr}\left(h_i^3 r \frac{d}{dr} p_i\right) = 0, \ i = 1, 2, 3.$$

The corresponding velocities and depth averaged velocities in each domain are

$$\mathbf{u}_i = -\frac{1}{2\mu}\frac{d}{dr}p_i \ \cdot z\,(h_i - z) \quad \Rightarrow \quad \mathbf{q}_i = \int_0^{h(r)} \mathbf{u}_i \, dz = -\frac{h_i^3}{12\mu}\frac{d}{dr}p_i, \ i = 1, 2, 3.$$

Region	1	2	3
Length of the region, L, mm	2	4,5	2
Maximum height, h_i^m, mm	0.7	0.1	0.1
$\epsilon = h_i^m / L$	0.35	0.022	0.05
ϵ^2	0.12	$4.94 \cdot 10^{-4}$	$2.5 \cdot 10^{-3}$
$\epsilon^2 Re$	$5.71 \cdot 10^{-4}$	$2.62 \cdot 10^{-5}$	$5.8 \cdot 10^{-5}$

TABLE 4.1: Characteristic values for each region of the posterior chamber

In this chapter we will introduce two different submodels for describing the flow. In the first one (§ 4.2) we will consider the hole in the lens to be of a finite size, whereas in the second model (§ 4.3) the hole is a point hole. The significant difference is that for the point-hole model we have to introduce the regularised pressure as we did for the case of iridotomy. We will observe that both models produce the same results.

4.2 Model with finite-size hole

We consider now the lens as the annulus $r_0 < r < r_l$. The inflow in the ciliary body is caused by aqueous production, and is equal to $F = 3\ \mu$l/min. Thus, on the outer boundary of the domain we have the condition $\frac{dp_1}{dr} = \frac{6\mu F}{\pi r_{pc} h_1^3},\ r = r_{pc}$. On the pupil we will impose zero pressure, $p_3 = 0,\ r = r_p$. We want the pressure to be continuous on the edge of the lens, $p_1 = p_2,\ p_1 = p_3$, in $r = r_l$ and the flux to be conserved $Q_2 + Q_3 = F$, where $Q_2,\ Q_3$ are the fluxes entering the regions 2 and 3 respectively. The last boundary condition is the one on r_0 and it is taken from Dagan's formula: $Q_2 = \pi \Delta p_2|_i r_0^4/(8S_l\mu + 3\pi r_0)$, where S_l is the thickness of the Hole-ICL and μ is dynamic viscosity.

Therefore, we can write the final equations considering the axisymmetric flow

$$\frac{d}{dr}\Big(h_i^3 r \frac{d}{dr} p_i\Big) = 0,\ i = 1, 2, 3 \tag{4.2.1}$$

$$\frac{dp_1}{dr} = \frac{6\mu F}{\pi r_{pc} h_1^3} \qquad \text{flux boundary condition on } r = r_{pc} \tag{4.2.2}$$

$$p_3 = 0 \qquad \text{on } r = r_p \tag{4.2.3}$$

$$\frac{r_0^4 \pi}{16\mu S + 3\mu\pi r_0} p_2 = \frac{\pi r_0 h_2^3}{6\mu} \frac{dp_2}{dr} \qquad \text{flux through the hole in the lens } r = r_0 \tag{4.2.4}$$

$$p_1 = p_2 \qquad \text{condition on } r = r_l \tag{4.2.5}$$

$$p_1 = p_3 \qquad \text{condition on } r = r_l \tag{4.2.6}$$

$$\frac{dp_2}{dr} \frac{\pi r_l h_2^3}{6\mu} + \frac{dp_3}{dr} \frac{\pi r_l h_3^3}{6\mu} = F \qquad \text{peservation of the flux on } r = r_l \tag{4.2.7}$$

Note that we assume h_2 is a constant, which makes sense considering the shape of Hole-ICL. For the case of linear domain (h_1 and h_3 are linear functions) we can obtain an analytical solution of the problem.

4.3 Model with a point hole

Now let us now consider the hole in the center of the ICL to be a point hole. For this case in order to avoid singularity at the point of the hole. As we did in 3.1.2 for the

iridotomy case, we will introduce the regularised pressure in the region 2

$$p_{2,reg} = p_2 - \frac{6\mu Q_0}{\pi h_2^3} \ln \frac{r}{r_0},$$

where r_h is the distance from the hole, which in our case coincides with the origin, so it is equal to r itself, and Q_0 is the flux through the hole. We can compute Q_0 using Dagan's formula: $Q_0 = \frac{r_0^4 \pi}{16\mu S + 3\mu\pi r_0} p_2|_0$. Then, the equation for $p_{2,reg}$ will be :

$$\frac{d}{dr}\Big(h_2^3 r \frac{d}{dr} p_{2,reg}\Big) = \frac{12\mu Q_0}{2\pi r} \frac{dh_2^3}{dr},$$

however, since we consider the height under the Hole-ICL h_2 to be a constant, we can simplify the above equations accordingly. We end up with the following final set of ODEs

$$\frac{d}{dr}\Big(r \frac{d}{dr} p_{2,reg}\Big) = 0, \qquad \frac{d}{dr}\Big(h_i^3 r \frac{d}{dr} p_i\Big) = 0, \ i = 1, 3. \tag{4.3.1}$$

The boundary conditions at zero are

$$p_{2,reg} = \frac{Q_0(16\mu S + 3\mu\pi r_0)}{r_0^4 \pi}, \qquad |p_{2,reg}| < \infty, \ r = 0 \tag{4.3.2}$$

and all other boundary conditions will remain the same as in § 4.2. Since h_2 is constant, we can compute $p_{2,reg}$ analytically, to get $p_{2,reg} = c_3 \ln r + c_4$. Because of the condition $|p_{2,reg}| < \infty$ we conclude that $c_3 = 0$. Constant c_4 we can define from (4.3.2). Thus, $p_{2,reg} = \frac{Q_0(16\mu S + 3\mu\pi r_0)}{r_0^4 \pi} \Rightarrow p_2 = \frac{Q_0(16\mu S + 3\mu\pi r_0)}{r_0^4 \pi} + \frac{6\mu Q_0}{\pi h_2^3} \ln \frac{r}{r_0}$. However, Q_0 is unknown still, and we can define it from the remaining boundary conditions which we rewrite in terms of the regularised pressure in region 2

$$\frac{dp_1}{dr} = \frac{6\mu Q}{\pi r_{pc} h_1^3} \qquad \text{flux boundary condition on } r = r_{pc} \tag{4.3.3}$$

$$p_3 = 0 \qquad \text{on } r = r_p \tag{4.3.4}$$

$$p_1 = p_{2,reg} + \frac{12\mu Q_0}{2\pi h_2^3} \ln \frac{r}{r_0} \qquad \text{condition on } r = r_l \tag{4.3.5}$$

$$p_1 = p_3 \qquad \text{condition on } r = r_l \tag{4.3.6}$$

$$\frac{dp_{2,reg}}{dr} \frac{\pi r_l h_2^3}{6\mu} + \frac{dp_3}{dr} \frac{\pi r_l h_3^3}{6\mu} = Q - Q_0 \qquad \text{peservation of the flux on } r = r_l \tag{4.3.7}$$

If h_1 and h_3 are linear functions we obtain an analytical solution of the equations (4.3.1) with boundary conditions (4.3.3)-(4.3.7). The results are shown in the § 4.4

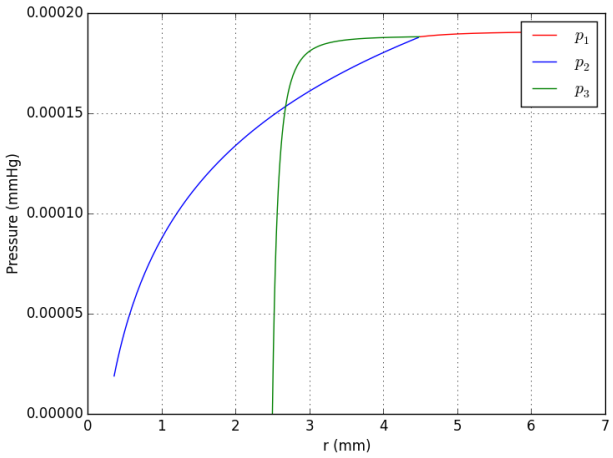

(a)

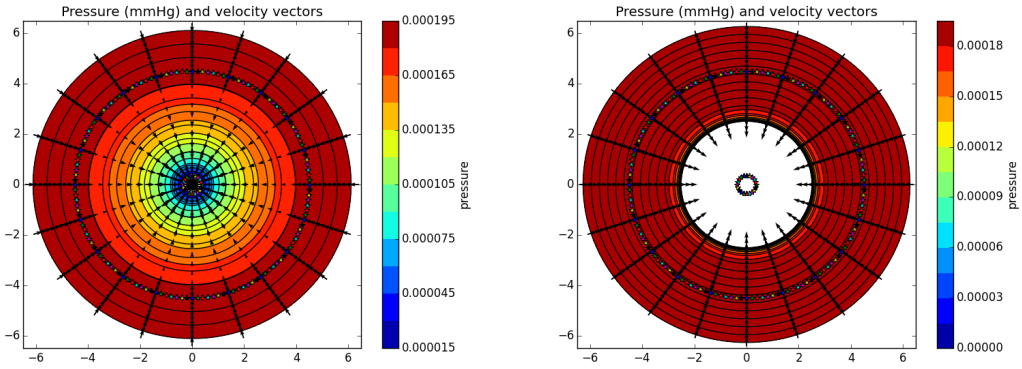

(b) (c)

FIGURE 4.3: Pressure (a) along the radial line and pressure distribution with average velocity vectors (b), (c), height under Hole-ICL is $h_2 = 0.2$mm

4.4 Results

In this section we will present the solution for models of the previous two sections. The solutions coincide, therefore we can use any of the two models. We solved the problem analitically for linear h_3 and h_1. In h_3 we defined the height of iris-Hole-ICL channel to be the same height as the iris-lens channel without Hole-ICL, equal to 7μm. The height below the Hole-ICL is not known, thus we tried different cases. The size of the hole in the lens is $r_0 = 0.36$mm, [1]. On the figure 4.3a the pressure distribution in the posterior chamber with the Hole-ICL implanted is shown. Each line represents pressure along the radial line in a different region: the red line represents the average pressure in region 1 (the outer region of the posterior chamber); the blue line - in region 2 (natural lens - Hole-ICL); the green one - in region 3 (Hole-ICL - iris). Figure 4.3b represents

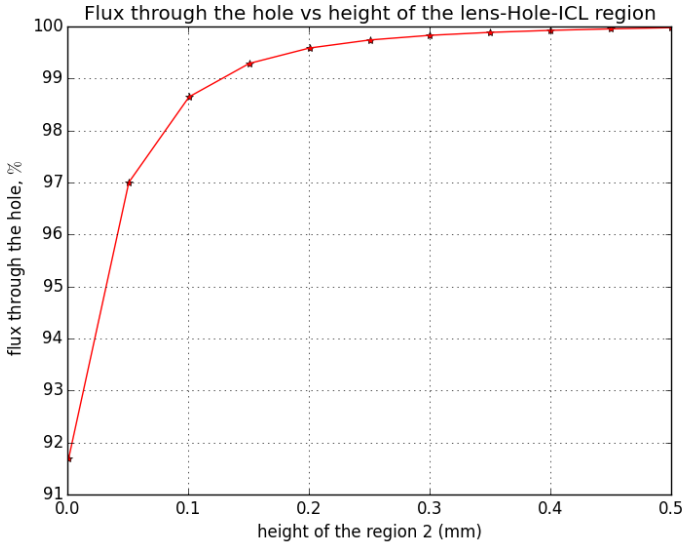

FIGURE 4.4: Flux through the hole vs height of the lens-Hole-ICL region

pressure distribution (colorbar) and average velocity vectors (arrows) in the regions 1-2. The view of the domain is from the top, the inner circle (with stars) is the hole in the Hole-ICL, the middle circle (with stars) is the edge of the Hole-ICL and the outer circle is the outer boundary of the posterior chamber. Similarly, the figure 4.3c shows the pressure distribution and the velocity profile in the regions 1-3. In this case the inner circle represents the pupil. The flux through the hole in the Hole-ICL 99.6% out of the total incoming flux produced by ciliary body. Note that he pressure here is 10 times smaller then in the case without the Hole-ICL.

Let us see what happens if we vary the height in the region 2 (under Hole-ICL) keeping the Hole-ICL - iris channel fixed and equal to 7μm. We think this is a reasonable assumption, since the iris "wants" to be on its original position without the implanted lens. On the figure 4.4 the flux percentage through the hole out of the total flux is shown as a function of the height of the region 2. We conclude that almost all the fluid flows out of the hole in the ICL.

4.5 Conclusions

In this section we proposed a preliminary model of circular Hole-ICL implanted into the posterior chamber of the eye. Two submodels were presented, one considering the hole in the ICL to be the hole of finite size and another one - with a point hole. The results

for both models are the same and they are presented in § 4.4. We conclude that almost all the flux goes out from the hole in the ICL, which is due to the fact that the channel iris-Hole-ICL is very small. We also conclude that the pressure is 10 times smaller with the lens than in the case without the lens. However, this conclusion might not be very reliable due to the lack of information about the geometry of the posterior chamber with the implanted lens.

As a proposed development of this model we can suggest first to consider a better geometry. Since the height of the domain has a strong impact on the behavior of the flow this might be a crucial improvement. High resolution ultrasound images with the lens implanted into the eye should work for measuring the height of the domain. Unfortunately, at the moment we do not have these data. Another improvement is to consider the real shape of the Hole-ICL. This will make the model much more complicated, since the flow and, what is more important, the domain, will no longer be axisymmetric. However, we assume that the overall picture of the results will not change significantly.

Chapter 5

Model of Hole-ICL with an iridotomy

5.1 Assumptions and mathematical model

The objective of current chapter is to combine the model of iridotomy with a model of Hole-ICL. We will start from the assumptions.

5.1.1 Assumptions

- **Geometry of the Hole-ICL:** We assume that the implanted lens is a circular plate of finite thickness S_l with radius r_l and a little hole in the center of radius r_0 (thisis the same geometry as considered in chapter 4).
- **Geometry of the posterior chamber:** We assume the posterior chamber has an axisymmetric shape. The domain is divided into 3 regions: region 1 without ICL, region 3anterior to the ICL and region 2 posterior to ICL. Each region has height $h_i(r),\ i = 1, 2, 3$, see fig. 4.2. The height of the region below the lens is constant, h_2 =const, and $h_1,\ h_3$ are linear functions. We need more data to overcome this assumption. The iridotomy is placed along positive x-axis in region 1 at a distance d_{hole} from the center of the pupil.
- **Geometry of iridotomy:** Where convenient we assume the iridotomy diameter is small enough that the iridotomy can be modelled as a point hole through the iris.

- **Flow through the hole:** As before, we use Dagan formula, for both the flow through the hole in the lens and the flow through iridotomy.

5.2 Mathematical model

We consider the basic model of an ICL lens in the posterior chamber with the iridotomy. We split the domain into 3 different regions with heights h_i. We will consider h_2 to be constant and h_1 and h_3 to be functions of the radius (see fig. 4.2). Using the model described in §4.1 for the region i we write the equation for the pressure p_i using lubrication theory

$$\boldsymbol{\nabla} \cdot (h_i^3 \boldsymbol{\nabla} p_i) = 0, \ i = 1, 2, 3. \tag{5.2.1}$$

Now let us consider the hole in the ICL and the iridotomy to be point holes with radius r_0 and a_i respectively. Then, we have to introduce the regularized pressure in regions 2 and 1 in order to avoid the singularity at the point of the hole, as we did for the iridotomy and the Hole-ICL model,

$$p_{1,reg} = p_1 - \frac{6\mu Q_i}{\pi h_i^3} \ln \frac{r_i}{a_i}.$$

$$p_{2,reg} = p_2 - \frac{6\mu Q_0}{\pi h_2^3} \ln \frac{r}{r_0},$$

where Q_0, Q_i denote the flux through the hole in the lens and the iridotomy respectively; and r_i is the distance from the iridotomy. We can compute Q_0 and Q_i using Dagan formula as before: $Q_0 = \frac{r_0^4 \pi}{8\mu S_l + 3\mu\pi r_0} p_2|_0$, $Q_i = \frac{a_i^4 \pi}{8\mu S_i + 3\mu\pi a_i} p_1|_0$, where S_l and S_i are thickness of Hole-ICL and the iris, respectively. The boundary conditions will be the same as in §4.2 with an additional condition at the point of the iridotomy. Therefore, the equations in terms of regularised pressure will become

$$\boldsymbol{\nabla} \cdot (h_1^3 \boldsymbol{\nabla} p_{1,reg}) = \frac{6\mu Q_i}{\pi r_i h_i^3} \frac{dh_1^3}{dr_i}, \tag{5.2.2}$$

$$\boldsymbol{\nabla} \cdot (\boldsymbol{\nabla} p_{2,reg}) = 0, \tag{5.2.3}$$

$$\boldsymbol{\nabla} \cdot (h_3^3 \boldsymbol{\nabla} p_3) = 0 \tag{5.2.4}$$

subject to the boundary conditions

$$p_{2,reg} = \frac{Q_0(8\mu S_l + 3\mu\pi r_0)}{r_0^4\pi} \qquad \text{the condition on flux in } r = 0 \tag{5.2.5}$$

$$\frac{\partial p_{1,reg}}{\partial r} = \frac{6\mu Q}{\pi r_{pc} h_1^3} - \frac{6\mu Q_i}{\pi r_i h_i^3}\frac{\partial r_i}{\partial r}. \qquad \text{flux boundary condition on } r = r_{pc} \tag{5.2.6}$$

$$p_3 = 0 \qquad \text{on } r = r_p \tag{5.2.7}$$

$$p_{1,reg} + \frac{6\mu Q_i}{\pi h_i^3}\ln\frac{r_i}{a_i} = p_{2,reg} + \frac{6\mu Q_0}{\pi h_2^3}\ln\frac{r}{r_0} \qquad \text{condition on } r = r_l \tag{5.2.8}$$

$$p_{1,reg} + \frac{6\mu Q_i}{\pi h_i^3}\ln\frac{r_i}{a_i} = p_3 \qquad \text{condition on } r = r_l \tag{5.2.9}$$

$$\frac{\partial p_{2,reg}}{\partial r}|_{r_l}\frac{r_l h_2^3}{12\mu} + \frac{\partial p_3}{\partial r}|_{r_l}\frac{r_l h_3^3}{12\mu} - \frac{\partial p_{1,reg}}{\partial r}|_{r_l}\frac{h_1^3 r_l}{12\mu} = \frac{Q_i h_1^3 r_l}{2\pi h_i^3 r_i}\frac{\partial r_i}{\partial r} - \frac{Q_0}{2\pi} \tag{5.2.10}$$

peservation of the flux on $r = r_l$

$$p_{1,reg} = \frac{Q_i(8\mu S_i + 3\mu\pi a_i)}{a_i^4\pi} \qquad \text{in the point of iridotomy} \tag{5.2.11}$$

Equations (5.2.2)-(5.2.11) describe the aqueous flow in the posterior chamber with implanted Hole-ICL and iridotomy.

5.3 Results

We will use the finite difference method for solving the equations (5.2.2)-(5.2.11). The used a scheme is based on the one described in § 3.2.1. Obviously, the method needs to be used for each $p_i,\ i = 1, 2, 3$. The boundary conditions (5.2.6), (5.2.10) were discretized using forward and backward second order finite differences. In this case the boundary conditions make it impossible to use the reduction or the modified reduction methods introduced in S 3.2.1.1. Thus we solve the linear system by storing everything into one matrix and then using a regular solver in Python from the package scipy.sparse.linalg.

The results are shown on the figure 5.1. This limits the size of the mesh that we can deal with. The size of the hole in the lens is $r_0 = 0.36$ mm. The iridotomy is placed along the positive x-axis at a distance 5mm from the center of the pupil. Figure 5.1a represents pressure distribution (colorbar) and average velocity vectors (arrows) in the regions 1-2. The view of the domain is from the top, the inner circle is the hole in the Hole-ICL, the middle circle is the edge of the Hole-ICL and the outer circle is the outer boundary of the posterior chamber. Similarly, figure 5.1b shows the pressure distribution and the velocity profile in the regions 1-3. In this case the inner circle represents the

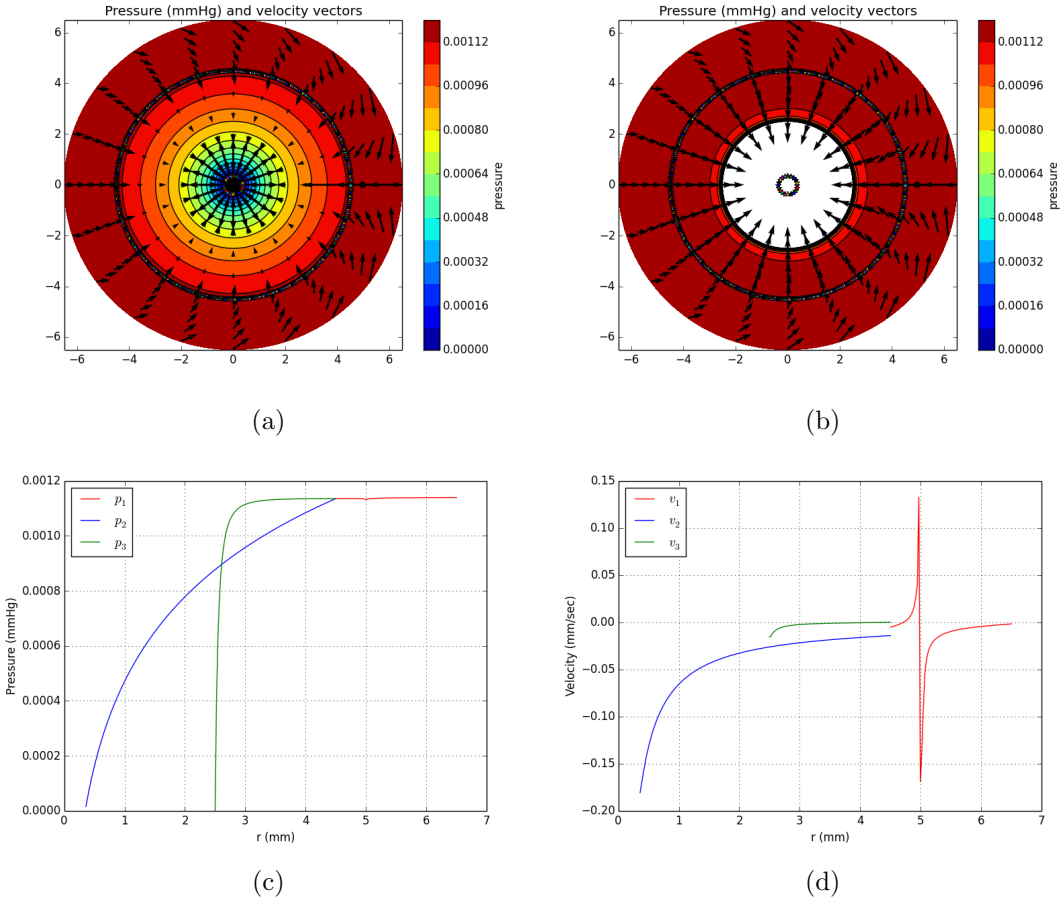

FIGURE 5.1: Pressure distribution and average velocity vectors for the radius of iridotomy 100μm

pupil. The flux through the iridotomy is 17% and the flux through the hole in the ICL is 81% out of the total incoming flux produced by ciliary body. In the figure 5.1c the pressure distribution in the posterior chamber with the Hole-ICL implanted is shown. Each line represents the pressure along the radial line in a different region: the red line represents the average pressure in region 1 (the outer region of the posterior chamber); the blue line - in region 2 (natural lens - Hole-ICL); the green one - in region 3 (Hole-ICL - iris). The plot 5.1d is the average velocity distribution along the radial line through the iridotomy in different regions.Note that the pressure is continuous from one region to another while the velocity is not. This is a consequence of the finite thickness of the ICL, which implies that the thickness of the region 1 is bigger that the sum of the height of regions 2 and 3.

We are interested in how the flow will change depending on the size of the iridotomy and the height of the domain under the Hole-ICL. In the figure 5.2a we plotted the flux

through the hole for different sizes of iridotomy. The height of the region under the Hole-ICL is 0.1 mm. We observe that even for large iridotomies (100 μm) almost all

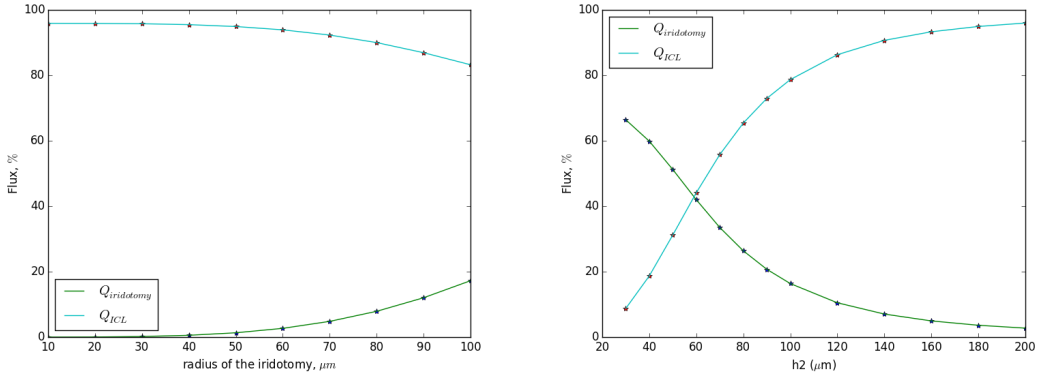

(a) (b)

FIGURE 5.2: Flux through the iridotomy and flux through the hole in ICL vs size of the iridotomy (a) and height of the region under the Hole-ICL (b)

the flux goes through the hole in the ICL. This could be explained by the fact that the height of the domain 2 is large (which is usually even larger according to [1]) and also the size of the hole in the lens is much bigger than the one of the iridotomy. Figure 5.2b is obtained by varying height of the domain under the Hole-ICL from 30 μm to 200 μm and keeping iridotomy large (100 μm). The majority of the fluid goes out of the iridotomy for small height (< 60 μm) and the flux decreasing rapidly with the increasing of the height. Therefore, we conclude that the flux through the iridotomy is significant only for the small height of the region 2.

5.4 Conclusions

In this chapter we combined the model aqueous flow in the posterior chamber in cases of Hole-ICL and iridotomy. The solution is obtained by using the finite difference method. From the results we observe that the iridotomy has a significant influence on the flow only when the height of the domain under the Hole-ICL is small. Note that, this is the conclusion for quite large iridotomy, for smaller holes the impact of the iridotomy is even less. Therefore, we might conclude that iridotomy might be useful only when the region between Hole-ICL and the natural crystalline lens gets very thin. However, this conclusion needs a verification due to the fact that geometry of the domain is not very realistic.

First improvement of the model will be to consider realistic geometry for the shape of the posterior chamber and the Hole-ICL. Another possible extension will be to consider the flow due to miosis.

Chapter 6

Conclusions

In this thesis we proposed a mathematical model of the aqueous flow in the posterior chamber of the eye. Two problems were considered: the iridotomy model and the model with implanted Hole-ICL. In both cases we use lubrication theory to obtain semi-analytical solutions.

For the problem of iridotomy, we separated cases of the flow caused by aqueous production and the flow caused by miosis (pupil contraction). For miosis we use quasi-steady approach by keeping the domain fixed and imposing velocities on the iris. We modelled an iridotomy as a point hole and assumed that the flux through the hole is proportional to the pressure drop across the hole. Moreover, we worked in terms of regularized pressure. For solving the equations we used a second order central finite difference scheme and for solving the corresponding linear system the modified method of reduction. Therefore, we obtained the solution for the pressure and velocity profile in the posterior chamber. For all the simulations we used a realistic geometry of the posterior chamber obtained by analysing a medical image. The results suggest, that iridotomy should have radius of least 40 μm to cause a significant impact on the flow. Moreover, in case of pupillary block the pressure grows so drastically, that one needs an iridotomy of at least 40 μm in radius in order to normalize the pressure. The position of the iridotomy and the velocity imposed on the iris do not have a big impact on the flux percentage through the hole. During miosis one has to avoid high velocity of the jet through the hole in order to prevent cells detachment from cornea. We found that the jet velocity is maximum for a radius of the hole of 60 μm. To improve the model, we need more data to model the velocity imposed on the iris and medical images of the posterior chamber with very high resolution.

For the model of Hole-ICL we used an axisymmetric shape of the domain. We split the posterior chamber into tree different regions (the region without ICL, the region above ICL and the region below the ICL) and applied lubrication theory to each of them. At the edge of the lens we imposed the continuity of pressure and conservation of flux. The pressure drop through the hole in ICL was modelled using Dagan's formula. For linear height of the domain we obtained an analytical solution of the problem. The results suggest that almost all the fluid exits through the hole in the lens, which is due to the fact that channel iris-Hole-ICL is very thin. The first improvement of the model will be to consider realistic geometry of the posterior chamber with implanted Hole-ICL. Secondly, we should consider the real shape of Hole-ICL for more accurate results.

The last part of the thesis combines the models of ICL and iridotomy. We place the iridotomy in the region without the lens and introduce regularized pressure in region without the lens (due to iridotomy) and region between the natural lens and Hole-ICL (due to the hole in ICL). Therefore, we obtain a set of equations which we solve using second order finite difference scheme. The results vary with the height of the region under the Hole-ICL. For the small height (~ 60 μm) most of the flux goes out from iridotomy, whereas for bigger height the flux through the iridotomy is not significant. We also observe that the size of iridotomy should also be large, since small iridotomies will not have significant impact on the flow. Therefore, the conclusion is that the iridotomy in case of implanted ICL should be large and performed for the case when the height between lens and Hole-ICL is small.

For further research we will suggest, firstly, to consider better geometry, especially in the case of ICL. Moreover, one may include in the model time dependence instead of considering the steady approach, especially in the case of miosis. Furthermore, combining this model with the model of the flow in the anterior chamber could be a good extension, which will result in the complete solution of the problem of aqueous humor flow in the anterior part of the eye.

Appendix A

Codes

In this appendix a brief outlook of the code for iridotomy problem is provided.

Main Program

```
import numpy as np
from closest_point import *
from newreduction import *
import geometry
from matrices import *
from velocities import *
ahole=5e-5#radius of iridotomy, m
dhole=5e-5#place of iridotomy, m
S=0.406e-3#thickness of the iris, m
mu=0.75e-3#viscosity kg/m/s
#set height of the domain
h=geometry()
#number of points in theta
n=10
nth=2**n
#partition of theta
th=np.arange(0,nth+1)/float(nth)*2*math.pi
dth=2*math.pi/float(nth)
#setting step in r and partition in r
s=[rpupil*dth]
r=[rpupil]
i=0
```

```
while r[i]<rpost:
    r=np.append(r,r[i]+s[i])
    s=np.append(s,(s[i]+r[i])*dth)
    i=i+1
nr=np.size(r)-1
r[nr]=rpost
s[nr-1]=r[nr]-r[nr-1]

#point closes to the point of the hole
istar=closest_node(dhole,r)

TH,R=np.meshgrid(th,r)
#set the matrices
C,F,D=matrices(ahole,dhole,nth,nr,h)

#use reduction to find preg
preg=newreduction(C,F,D,n,nr,istar)

#Dagan formula for the flux through the hole
Qhole=np.pi*ahole**4/(8*S*mu+3*mu*np.pi*ahole)*preg[istar,0]
#from the regularized pressure to the pressure
p=preg+3*mu*Qhole/np.pi/h[istar]**3*np.log((np.multiply(R,R)+\
dhole**2-2*R*dhole*np.cos(TH))/ahole**2)

#velocity components
qr,qtheta=velocities(p)
```

Bibliography

[1] Takushi Kawamorita, Hiroshi Uozato, and Kimiya Shimizu. Fluid dynamics simulation of aqueous humour in a posterior-chamber phakic intraocular lens with a central perforation. *Graefe's archive for clinical and experimental ophthalmology*, 250(6):935–939, 2012.

[2] J. J. Heys, V. H. Barocas, and M. J. Taravella. Modeling passive mechanical interaction between aqueous humor and iris. *Transactions of the ASME*, 123:540–547, December 2001.

[3] C. R. Canning, M. J. Greaney, J. N. Dewynne, and A. Fitt. Fluid flow in the anterior chamber of a human eye. *IMA Journal of Mathematics Applied in Medicine and Biology*, 19:31–60, 2002.

[4] SeyedAmirreza Modarreszadeh, Omid Abouali, Alireza Ghaffarieh, and Goodarz Ahmadi. Physiology of aqueous humor dynamic in the anterior chamber due to rapid eye movement. *Physiology & behavior*, 2014.

[5] Omid Abouali, Amirreza Modareszadeh, Alireza Ghaffarieh, and Jiyuan Tu. Investigation of saccadic eye movement effects on the fluid dynamic in the anterior chamber. *Journal of biomechanical engineering*, 134(2):021002, 2012.

[6] D. M. Silver and H. A. Quigley. Aqueous flow through the iris-lens channel: estimates o the differential pressure between the anterior and the posterior chambers. *J. Glaucoma*, 13(2):100–107, April 2004.

[7] Jennifer H Siggers and C Ross Ethier. Fluid mechanics of the eye. *Annual Review of Fluid Mechanics*, 44:347–372, 2012.

[8] Sergio Kwitko and Andressa Prestes Stolz. Iris-claw (artisan®/artiflex®) phakic intraocular lenses for high myopia and high hyperopia. 2011.

[9] Martin Baumeister, Jens Bühren, and Thomas Kohnen. Position of angle-supported, iris-fixated, and ciliary sulcus–implanted myopic phakic intraocular lenses evaluated by scheimpflug photography. *American journal of ophthalmology*, 138(5):723–731, 2004.

[10] T Kohnen, M Baumeister, and M Cichocki. Intraokularlinsen zur korrektur von refraktionsfehlern. *Der Ophthalmologe*, 102(10):1003–1018, 2005.

[11] Rodolfo Repetto, Jan O Pralits, Jennifer H Siggers, and Paolo Soleri. Phakic iris-fixated intraocular lens placement in the anterior chamber: Effects on aqueous flowphakic iris-fixated intraocular lens placement. *Investigative Ophthalmology & Visual Science*, 56(5):3061–3068, 2015.

[12] Kazutaka Kamiya, Kimiya Shimizu, Daisuke Aizawa, Akihito Igarashi, Mari Komatsu, and Akio Nakamura. One-year follow-up of posterior chamber toric phakic intraocular lens implantation for moderate to high myopic astigmatism. *Ophthalmology*, 117(12):2287–2294, 2010.

[13] Donald R Sanders, David Schneider, Robert Martin, David Brown, David Dulaney, John Vukich, Stephen Slade, and Steven Schallhorn. Toric implantable collamer lens for moderate to high myopic astigmatism. *Ophthalmology*, 114(1):54–61, 2007.

[14] Li-Ju Chen, Yun-Jau Chang, Jonathan C Kuo, Rama Rajagopal, and Dimitri T Azar. Metaanalysis of cataract development after phakic intraocular lens surgery. *Journal of Cataract & Refractive Surgery*, 34(7):1181–1200, 2008.

[15] Kunitoshi Fujisawa, Kimiya Shimizu, Shigekazu Uga, Masanobu Suzuki, Koichi Nagano, Yuuki Murakami, and Hiroko Goseki. Changes in the crystalline lens resulting from insertion of a phakic iol (icl) into the porcine eye. *Graefe's Archive for Clinical and Experimental Ophthalmology*, 245(1):114–122, 2007.

[16] Zeev Dagan, Sheldon Weinbaum, and Robert Pfeffer. An infinite-series solution for the creeping motion through an orifice of finite length. *Journal of Fluid Mechanics*, 115:505–523, 1982.

[17] Alexandr Samarskiy and Evgeniy Nikolaev. Methods for solving grid equations. pages 73–76,154–156,569–577, 1978.

[18] Yuichi Kaji, Tetsuro Oshika, Tomohiko Usui, and Jun Sakakibara. Effect of shear stress on attachment of corneal endothelial cells in association with corneal endothelial cell loss after laser iridotomy. *Cornea*, 24(8):S55–S58, 2005.